

RESEARCH ARTICLE

Robust successive generalised dynamic inversion control of satellite launch vehicles

A.H. Bajodah¹ and U. Ansari²

Aerospace Engineering Department, King Abdulaziz University, Jeddah, Saudi Arabia

Corresponding author: A.H. Bajodah; Email: abajodah@kau.edu.sa

Received: 8 November 2023; **Revised:** 5 October 2024; **Accepted:** 18 November 2024

Keywords: Generalized Dynamic Inversion Control; Robust Control; Satellite Launch Vehicle; Trajectory Optimization; Lyapunov Stability

ABSTRACT

In this paper, we design a robust Successive Generalised Dynamic Inversion (SGDI) flight control system for high-performance trajectory tracking of target sun-synchronous orbit Satellite Launch Vehicles (SLVs). The robust SGDI control system is designed to track an optimal reference trajectory such that the desired orbital terminal conditions of the ascent flight phase are achieved. The proposed SGDI is composed of two loops. The attitude control loop employs Dynamically Scaled Generalised Inversion (DSGI) of Servo Constraint Dynamics (SVD) in the deviations of Euler attitude angles from their desired optimal trajectories. The inner-dynamics control loop employs DSGI of an SVD in the SLV angular velocity components. Robustification control elements are augmented within the two loops of the baseline SGDI control system to overcome control performance degradation due to dynamic scaling of the Moore-Penrose generalised inverse, modeling and parametric uncertainties, and exogenous disturbances. The robust SGDI control system works to enforce global convergence of the SLV attitude trajectories to the reference trajectories. The high-performance attributes of the robust SGDI control system are verified via comparisons with a classical sliding mode control system, and by performing numerous runs of Monte Carlo simulations under various types of uncertainties and external wind disturbances.

Nomenclature

h	altitude
h_{ref}	reference altitude
V	velocity
V_{ref}	reference velocity
p	roll rate
q	pitch rate
r	yaw rate
\mathbf{X}	displacement vector
\mathbf{V}	velocity vector
\mathbf{e}	error vector
\mathbf{g}	acceleration due-to-gravity vector
m	mass
T	thrust
D	drag
Q	dynamic pressure
S_{ref}^*	reference surface area
C_D	drag coefficient
C_{L_α}	lift coefficient derivative with respect to α
C_{L_β}	lift coefficient derivative with respect to β

\mathcal{L}	aerodynamic and propulsive moment vector about body x axis
\mathcal{M}	aerodynamic and propulsive moment vector about body y axis
\mathcal{N}	aerodynamic and propulsive moment vector about body z axis
J_x	moment of inertia about body x axis
J_y	moment of inertia about body y axis
J_z	moment of inertia about body z axis
$S^\times(\cdot)$	skew symmetric cross product matrix
C_{m_x}	pitching moment coefficient about body x axis
l	vehicle length
R_e	Earth's equatorial radius
R_L	local Earth's radius
b_{rud}	distance between centre of motor and vehicle's longitudinal axis
X_{cg}	distance from the vehicle's nose to its centre of mass
X_{cp}	distance from the vehicle's nose to its centre of pressure
X_{rud}	distance from the vehicle's nose to the motor's hinge line
\mathcal{P}	null projection matrix

Greek symbol

ϑ	flight path angle
ϑ_{ref}	reference flight path angle
α	angle-of-attack
σ	heading angle
β	side slip angle
ϕ	roll angle
θ	pitch angle
ψ	yaw angle
ϑ_l	local flight path angle
ω_e	Earth's rotational speed
δ_ϕ	roll control deflection
δ_θ	pitch control deflection
δ_ψ	yaw control deflection
λ	latitude
ξ	attitude error deviation function
η	null control vector
ν	dynamic scaling factor
ζ	body rate deviation function
Δ	attitude corrections
ϵ_y	normal positional error
ϵ_z	lateral positional error
∇	thrust offset
ϱ	thrust misalignment

1.0 Introduction

The attitude control system design for Satellite Launch Vehicles (SLVs) has been an active area of research for the last three decades. The factors that make it challenging to design a robust SLV flight control system include the highly complex nonlinear SLV dynamics, the big variations in aerodynamic loads and propulsive forces throughout the flight envelope, inertia and aerodynamic parametric uncertainties of the SLV, in addition to wind and other exogenous disturbances that the SLV may be exposed to.

The vast majority of practical control system designs that were proposed initially for SLVs were linear. To overcome SLV control performance degradations that result from neglecting high nonlinearities in the SLV dynamics, gain scheduling of the linear control system parameters were used to be implemented

[1–4]. However, gain scheduling methods are costly and became needless with the recent advancements in nonlinear control systems.

The focus has been shifting during the last two decades towards designing modern SLV control systems that overcome the limitations of classical linear control systems and the complexity of gain scheduling. A variety of nonlinear control system methodologies are now found in the SLV control literature, e.g. dynamic inversion with backstepping control [5], Sliding Mode Control (SMC) [6], fault-tolerant control [7, 8], adaptive control [9, 10] and intelligent control [11–13].

Among the popular nonlinear control system design methodologies is global feedback linearisation via Nonlinear Dynamic Inversion (NDI). The NDI control law is designed to eliminate system nonlinearities by means of feedback. As a consequence, well-established linear control techniques can be incorporated in the outer feedback control loop. In NDI, however, the linearised system is obtained by direct nonlinearity cancellation. Therefore, the methodology is heavily dependent on the mathematical model of the controlled system.

As a consequent, dynamic inversion errors of a poorly modeled plant dynamics degrade an NDI control system stability and performance by a big extent [14]. Numerous modifications were made to the NDI control system structure to improve its robustness [15–17]. However, some limitations of feedback linearisation via NDI remain problematic, including useful nonlinearities cancellations, large NDI control efforts, squaring assumptions and approximations of nonsquare controlled plants, and singularity configurations of the controlled system matrix.

Generalised Dynamic Inversion (GDI) [18–23] is a dynamic inversion control design methodology that avoids many disadvantages of classical NDI. The GDI control design methodology provides the ability of partial feedback linearisation of the closed loop dynamics, and it provides the flexibility of involving other control system design methodologies within the dynamic inversion framework, e.g. energy-based control techniques.

Therefore, the GDI control methodology avoids blind cancellation of plant nonlinearities and makes it possible to reduce the control effort that is required to execute dynamic inversion. Finally, the GDI control methodology is based on the nonsquare Moore-Penrose Generalised Inversion (MPGI) tool [24, 25]. Hence, GDI control bypasses the plant squaring assumptions and approximation tactics, and it is not affected by the controlled system square matrix singularity configurations.

The GDI control methodology is rooted in analytical dynamics [26], and it was inspired by the MPGI-based Greville formula [27, 28] for solving linear algebraic systems of equations. The GDI control law is composed of two cooperating control parts that act on two orthogonally complement control spaces: one part is a particular part that realises the dynamic constraints, and the other is an auxiliary part that is affine in a null control vector. Orthogonality of the particular and the auxiliary control subspaces guarantees noninterference of the two control actions, and thus it ensures that both actions work towards a unified goal, and work to reduce the total control effort.

A GDI nonlinear control system design begins by prescribing a desired Servo Constraint Dynamics (SVD) that encapsulates the GDI control design objectives. The SVD is generalised inverted for the control variables that realise that dynamics by using a modification of the Greville formula. The modified Greville formula is constructed by scaling the MPGI in the particular part of the formula by a dynamic factor. The Dynamically Scaled Generalised Inverse (DSGI) avoids MPGI singularity as the controlled system dynamics evolves. The nonempty nullspace of the nonsquare generalised-inverted matrix in the modified Greville formula is utilised to perform other objectives of the GDI control design, mainly for stabilising the inner dynamics of the closed loop GDI control system. The GDI control methodology has been applied to numerous aerospace engineering and robotics applications [18–23, 29–34].

The present paper extends the authors' previous works on SLV GDI control [29, 30]. The baseline GDI control methodology is modified by applying GDI control in a successive manner to design the null control vector in the auxiliary part of the GDI control law on top of its application to design the particular part of the GDI control law. The particular part of the Successive GDI (SGDI) control law employs GDI on an SVD in the SLV's Euler attitude angles, and it is responsible for controlling the SLV's outer dynamics. The auxiliary part of the SGDI control law employs GDI on an SVD in the SLV's angular velocity variables, and it is responsible for controlling the SLV's inner dynamics.

Due to the favourable geometry of the Greville formula, the order in which the attitude and the inner-dynamics loops closures is performed is irrelevant and can be performed arbitrarily to achieve the same SGDI closed loop dynamics. To enhance SGDI control performance robustness against SLV modeling uncertainties and exogenous disturbances and generalised inversion dynamic scaling, integral control elements are augmented within the attitude and the inner-dynamics loops of the baseline SGDI control system. The performance-robustifying control elements are augmented in a manner that maintains geometrical features of the nominal SGDI control law.

The proposed robust SGDI control system is validated by numerical simulations on a six Degrees Of Freedom (DOFs) simulator of a four-stage SLV subjected to inertial, aerodynamic and propulsive parametric uncertainties under unsteady wind effects. Moreover, the proposed control system is compared with a classical SMC control system, the second of which is known for its high, robust performance. Finally, diversified Monte-Carlo statistical simulations are carried out to verify robustness attributes of the SLV robust SGDI control system in the presence of internal perturbations and environmental disturbances.

In the realm of SLV attitude control systems, the major contribution of this article is threefold. First, a novel variant of GDI control is introduced for controlling the complex coupled nonlinear SLV attitude dynamics under environmental challenges. The control actions on the outer and inner SLV dynamics work synergistically without interference towards robust SLV attitude control. Second, a detailed Lyapunov stability-based analysis is presented to prove asymptotic convergence of the state variables to their optimal reference trajectories. Third, numerical simulations supported with diversified Monte-Carlo analysis are carried out to validate efficacy of SGDI control in the presence of model uncertainties and environmental disturbances.

The remaining part of the paper is organised as follows. Mathematical modeling of the SLV is presented in Section 2. Section 3 elucidates the baseline SGDI control system design, and Section 4 delves into SGDI control system robustification. Section 5 describes the optimal reference trajectory generation methodology, and elaborates the trajectory reshaping strategy and rational energy management. Numerical simulations of the proposed robust SGDI SLV control system are shown in Section 6, in addition to performance evaluation of the proposed system by comparisons with a SMC system and through Monte Carlo simulations. The paper is concluded in Section 7.

2.0 Six-DOFs mathematical modeling

In developing a mathematical model for the SLV's kinematics and dynamics, the Earth is assumed to be ellipsoidal, and its rotation together with the atmosphere is taken as a single frame of reference. The effect of Earth's rotation is also taken into account by modeling the Coriolis and the centrifugal accelerations. The synergy between the Earth and the SLV is modeled with the aid of the two-body problem formulation. The SLV's six DOFs kinematics is given by the following translational and rotational kinematical equations of motion [35]

$$\dot{\mathbf{X}}_l = \mathbf{V}_l, \quad (1)$$

$$\dot{\phi} = p + q \tan \psi \sin \phi + r \cos \phi \tan \psi \quad (2)$$

$$\dot{\theta} = q \sin \phi / \cos \psi + r \cos \phi / \cos \psi \quad (3)$$

$$\dot{\psi} = q \cos \phi - r \sin \phi. \quad (4)$$

In Equation (1), $\mathbf{X}_l = [x_l \ y_l \ z_l]^T$, where x_l , y_l , and z_l are the displacement vector components of the SLV from its launch site, expressed in the Launch Reference Frame (LRF), and $\mathbf{V}_l = [V_{x_l} \ V_{y_l} \ V_{z_l}]^T$, where V_{x_l} , V_{y_l} , and V_{z_l} are the velocity vector components of the SLV relative to the LRF. The SLV's three translational DOFs dynamical equations of motion are given by [35]

$$\dot{\mathbf{V}}_l = \frac{L_{lb}}{m} \begin{bmatrix} -QS_{\text{ref}}C_D + T \cos \delta_\phi \\ QS_{\text{ref}}C_{L\alpha} + 0.5T \sin \delta_\theta \\ QS_{\text{ref}}C_{L\beta} + 0.5T \sin \delta_\psi \end{bmatrix} + L_{le}\mathbf{g}_e - L_{le}\Omega_e^\times \Omega_e^\times \mathbf{X}_e - 2L_{le}\Omega_e^\times \mathbf{V}_e. \tag{5}$$

In Equation (5), $\mathbf{X}_e = [x_e \ y_e \ z_e]^T$, where $x_e, y_e,$ and z_e are the displacement vector components of the SLV from its launch site, expressed in the earth-fixed Geocentric Reference Frame (GRF), and $\mathbf{V}_e = [V_{x_e} \ V_{y_e} \ V_{z_e}]^T$, where $V_{x_e}, V_{y_e},$ and V_{z_e} are the SLV's velocity vector components relative to the GRF. Similarly, $\mathbf{g}_e = [g_{x_e} \ g_{y_e} \ g_{z_e}]^T$, where $g_{x_e}, g_{y_e},$ and g_{z_e} are the acceleration-due-to gravity vector components in the GRF. The variable Ω_e^\times denotes the skew symmetric cross product matrix of the vector $\Omega_e = [0 \ 0 \ \omega_e]^T$, and is given by

$$\Omega_e^\times = \begin{bmatrix} 0 & -\omega_e & 0 \\ \omega_e & 0 & 0 \\ 0 & 0 & 0 \end{bmatrix}, \tag{6}$$

The matrices $L_{lb}, L_{le} \in \mathbb{R}^{3 \times 3}$ are the transformation matrices from the Body-fixed Reference Frame (BRF) to the LRF and from the GRF to the LRF, respectively. Also, The SLV's three rotational DOFs dynamical equations of motion in the SLV's BRF are given by [35]

$$\dot{p} = \mathcal{L}/J_x \tag{7}$$

$$\dot{q} = (J_z - J_x) pr/J_y + \mathcal{M}/J_y \tag{8}$$

$$\dot{r} = -\frac{(J_y - J_x) pq}{J_z} + \frac{\mathcal{N}}{J_z}, \tag{9}$$

$$\theta = \vartheta + \alpha, \quad \psi = \sigma + \beta. \tag{10}$$

The moment components $\mathcal{L}, \mathcal{M},$ and \mathcal{N} in Equations (7)–(10) are composed of aerodynamic moments, control moments and disturbance moments due to thrust misalignment [35]. The aerodynamic moment components in the BRF are given by Equations (11)–(13)

$$\mathcal{L}_a = QS_{\text{ref}}lC_{m_x} \tag{11}$$

$$\mathcal{M}_a = -QS_{\text{ref}}C_{L\alpha} \alpha (X_{cp} - X_{cg}), \tag{12}$$

$$\mathcal{N}_a = QS_{\text{ref}}C_{L\beta} \beta (X_{cp} - X_{cg}). \tag{13}$$

The control moments in the BRF are given by Equations (14)–(16)

$$\mathcal{L}_\delta = Tb_{\text{rud}}\delta_\phi \tag{14}$$

$$\mathcal{M}_\delta = \frac{1}{2}T (X_{\text{rud}} - X_{\text{cg}}) \delta_\theta, \tag{15}$$

$$\mathcal{N}_\delta = \frac{1}{2}T (X_{\text{rud}} - X_{\text{cg}}) \delta_\psi. \tag{16}$$

Finally, the moments caused by disturbances due to misalignment of the thrust vector ρ from the SLV's centre of mass are caused by the thrust offset ∇ relative to the centre of mass, and are expressed in the BRF as seen in Equations (17)–(19)

$$\mathcal{L}_\varrho = T \sin(\varrho) \nabla_T, \tag{17}$$

$$\mathcal{M}_\varrho = \frac{1}{2} T \sin(\varrho) (X_{rud} - X_{cg}) + \frac{1}{2} T \nabla_T, \tag{18}$$

$$\mathcal{N}_\varrho = \frac{1}{2} T \sin(\varrho) (X_{rud} - X_{cg}) + \frac{1}{2} T \nabla_T. \tag{19}$$

By combining the moment components about each BRF axis as given by Equations (11)–(19), the following expressions for aerodynamic, propulsive and thrust misalignment moment components are obtained

$$\mathcal{L} = QS_{ref}lC_{m_x} + Tb_{rud}\delta_\phi + T \sin(\varrho) \nabla_T \tag{20}$$

$$\mathcal{M} = -QS_{ref}C_{L_\alpha} \alpha (X_{cp} - X_{cg}) + 0.5T (X_{rud} - X_{cg}) \delta_\theta + 0.5T \sin(\varrho) (X_{rud} - X_{cg}) + 0.5T \nabla_T, \tag{21}$$

$$\mathcal{N} = QS_{ref}C_{L_\beta} \beta (X_{cp} - X_{cg}) + 0.5T (X_{rud} - X_{cg}) \delta_\psi + 0.5T \sin(\varrho) (X_{rud} - X_{cg}) + 0.5T \nabla_T. \tag{22}$$

Let the attitude state vector of the SLV be defined as $\mathbf{x} = [\phi \ \theta \ \psi \ p \ q \ r]^T$, and let the control vector of the SLV be defined as $\mathbf{u} = [\delta_\phi \ \delta_\theta \ \delta_\psi]^T$. Also, let the state vector \mathbf{x} be partitioned as

$$\mathbf{x}_o = [\phi \ \theta \ \psi]^T, \quad \mathbf{x}_i = [p \ q \ r]^T \tag{23}$$

where \mathbf{x}_o is the vector of outer (unactuated) attitude state variables, and \mathbf{x}_i is the vector of inner (actuated) angular velocity state variables. Hence, the unactuated attitude dynamics given by Equations (2), (3) and (4) may be written compactly as

$$\dot{\mathbf{x}}_o = H(\mathbf{x}_o) \mathbf{x}_i \tag{24}$$

where

$$H(\mathbf{x}_o) = \begin{bmatrix} 1 & \tan \psi \sin \phi & \cos \phi \tan \psi \\ 0 & \sin \phi / \cos \psi & \cos \phi / \cos \psi \\ 0 & \cos \phi & -\sin \phi \end{bmatrix}. \tag{25}$$

Also, the actuated inner velocity dynamics given by Equations (7), (8) and (9) can be written compactly as

$$\dot{\mathbf{x}}_i = -J^{-1}S^\times(\mathbf{x}_i) J\mathbf{x}_i + J^{-1}\mathbf{M} \tag{26}$$

where $S^\times(\mathbf{x}_i)$ is given by

$$S^\times(\mathbf{x}_i) = \begin{bmatrix} 0 & -r & q \\ r & 0 & -p \\ -q & p & 0 \end{bmatrix} \tag{27}$$

In Equation (26), $J = \text{diag}(J_x, J_y, J_z)$ is the diagonal matrix containing J_x , J_y , and J_z in its diagonal entries, and $\mathbf{M} = [\mathcal{L} \ \mathcal{M} \ \mathcal{N}]^T$. Substituting the expressions given by Equations (20), (21) and (22) in Equation (26) yields

$$\dot{\mathbf{x}}_i = -J^{-1}S^\times(\mathbf{x}_i) J\mathbf{x}_i + J^{-1}QS_{ref}\mathbf{f}(\alpha, \beta) + J^{-1}\mathbf{G}\mathbf{u} \tag{28}$$

where

$$\mathbf{f}(\alpha, \beta) = \begin{bmatrix} lC_{m_x} \\ -C_{L_\alpha} \alpha (X_{cp} - X_{cg}) \\ C_{L_\beta} \beta (X_{cp} - X_{cg}) \end{bmatrix}, \tag{29}$$

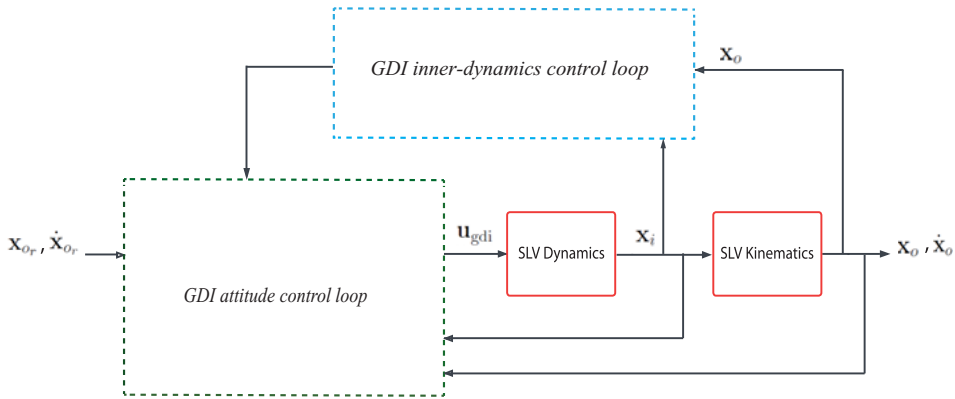


Figure 1. General SGDI control system structure: the inner loop controls SLV’s internal dynamics, and the outer loop controls SLV’s attitude dynamics.

$$G = \begin{bmatrix} Tb_{rud} & 0 & 0 \\ 0 & 0.5T(X_{rud} - X_{cg}) & 0 \\ 0 & 0 & 0.5T(X_{rud} - X_{cg}), \end{bmatrix}, \tag{30}$$

and

$$\mathbf{u} = [\delta_\phi \quad \delta_\theta \quad \delta_\psi]^T. \tag{31}$$

Finally, Equation (28) is rewritten more compactly as

$$\dot{\mathbf{x}}_i = \mathbf{A} + \mathbf{B}\mathbf{u} \tag{32}$$

where

$$\mathbf{A} = -J^{-1}S^\times(\mathbf{x}_i)J\mathbf{x}_i + J^{-1}QS_{ref}\mathbf{f}(\alpha, \beta), \tag{33}$$

and B is the full-rank control influence matrix given by

$$B = J^{-1}G. \tag{34}$$

3.0 Baseline SGDI feedback control system design

The SGDI control system is the backbone of the proposed robust SGDI control system. The SGDI control system is composed of two GDI control loops as illustrated in Fig. 1. The guidance system feeds the reference attitude trajectories to the GDI attitude control loop, which works to control the attitude dynamics given by Equation (24) such that the attitude variables track the reference attitude trajectories. The GDI inner-dynamics control loop works to stabilise the inner (angular velocity) dynamics of the SLV given by Equation (26).

3.1 GDI attitude control loop design

The first step in designing the attitude control loop of the baseline SGDI control system is to prescribe a time differential SVD that resembles the SLV’s desired attitude trajectories deviation dynamics from their desired trajectories. Hence, the outer (attitude) error vector is defined as

$$\mathbf{e}_o = \mathbf{x}_o - \mathbf{x}_{o_r}(t), \tag{35}$$

where $\mathbf{x}_{or}(t) = [\phi_r(t) \ \theta_r(t) \ \psi_r(t)]^T$ is a bounded twice differentiable reference attitude angles vector function. The attitude error deviation function is defined as

$$\xi = \frac{1}{2} \mathbf{e}_o^T K_o \mathbf{e}_o \tag{36}$$

where $K_o \in \mathbb{R}^{3 \times 3}$ is a positive definite constant matrix such that ξ vanishes if and only if the attitude state trajectories converge to the corresponding desired attitude state trajectories. To fulfill that purpose, an asymptotically stable SVD in ξ is prescribed and is enforced by means of GDI control. The SVD takes the following Linear Time Invariant (LTI) form

$$\ddot{\xi} + a_1 \dot{\xi} + a_2 \xi = 0, \quad a_1 > 0, \ a_2 > 0 \tag{37}$$

where the order (two) of the SVD is equal to of the relative degree of ξ with respect to \mathbf{u} , such that $(\xi, \dot{\xi}) = 0_2$ is globally asymptotically stable [20]. The first and second time derivatives of ξ are

$$\dot{\xi} = \mathbf{e}_o^T K_o \dot{\mathbf{e}}_o \tag{38}$$

and

$$\ddot{\xi} = \mathbf{e}_o^T K_o (\Delta_o + H(\mathbf{x}_o) \mathbf{B} \mathbf{u}) + \dot{\mathbf{e}}_o^T K_o \dot{\mathbf{e}}_o \tag{39}$$

where

$$\dot{\mathbf{e}}_o = H(\mathbf{x}_o) \mathbf{x}_i - \dot{\mathbf{x}}_{or}, \tag{40}$$

and

$$\Delta_o = H(\mathbf{x}_o) \mathbf{A} + \dot{H}(\mathbf{x}_o, \mathbf{x}_i) \mathbf{x}_i - \dot{\mathbf{x}}_{or} \tag{41}$$

such that $\dot{H}(\mathbf{x}_o, \mathbf{x}_i)$ is the element-wise time derivative of $H(\mathbf{x}_o)$. By substituting the time derivatives given by Equations (38) and (39) in the SVD given by Equation (37), the differential form of the SVD is converted to the following algebraic form

$$\mathcal{A}_o \mathbf{u} = \mathcal{B}_o, \tag{42}$$

where

$$\mathcal{A}_o = \mathbf{e}_o^T K_o H(\mathbf{x}_o) \mathbf{B} \tag{43}$$

and

$$\mathcal{B}_o = -\mathbf{e}_o^T K_o \Delta_o - \dot{\mathbf{e}}_o^T K_o \dot{\mathbf{e}}_o - a_1 \dot{\xi} - a_2 \xi. \tag{44}$$

Equation (42) is over-determined in \mathbf{u} and is consistent for all $\mathbf{e}_o \neq 0_3$. Therefore, Equation (42) has infinite number of solutions. The solutions for \mathbf{u} are parameterised by an arbitrary outer null control vector $\eta_o \in \mathbb{R}^3$ in the MPGI-based Greville formula as

$$\mathbf{u} = \underbrace{\mathcal{A}_o^+ \mathcal{B}_o}_{\in \mathcal{R}(\mathcal{A}_o^T)} + \underbrace{\mathcal{P}_o \eta_o}_{\in \mathcal{N}(\mathcal{A}_o)}, \tag{45}$$

where \mathcal{A}_o^+ is the MPGI of \mathcal{A}_o , and is given as

$$\mathcal{A}_o^+ = \begin{cases} \mathcal{A}_o^T / (\mathcal{A}_o \mathcal{A}_o^T) & \mathcal{A}_o \neq 0_{1 \times 3} \\ 0_3 & \mathcal{A}_o = 0_{1 \times 3} \end{cases} \tag{46}$$

and \mathcal{P}_o is the null projection matrix on the nullspace of \mathcal{A}_o , and is given by

$$\mathcal{P}_o = \mathbf{I}_{3 \times 3} - \mathcal{A}_o^+ \mathcal{A}_o. \tag{47}$$

The control vector \mathbf{u} is composed of a particular part $\mathcal{A}_o^+ \mathcal{B}_o$ and an auxiliary part $\mathcal{P}_o \eta_o$. The particular part of \mathbf{u} acts on the range space $\mathcal{R}(\mathcal{A}_o^T)$, and it works to enforce the SVD given by Equation (42). The auxiliary part of \mathbf{u} acts on the orthogonally complement nullspace $\mathcal{N}(\mathcal{A}_o)$ such that $rank(\mathcal{A}_o^T) + rank(\mathcal{P}_o) = \dim(\mathbf{u}) = 3$. The value of η_o does not affect the SVD enforcement because the

null projection matrix \mathcal{P}_o projects η_o on $\mathcal{N}(\mathcal{A}_o)$. The vector η_o is designed to stabilise the inner dynamics of the SLV as shown later in the paper. Because \mathcal{A}_o^+ is a nonzero single column matrix, it follows that $rank(\mathcal{P}_o) = \dim(\mathbf{u}) - rank(\mathcal{A}_o^+) = 3 - 1 = 2$. However, the MPGI \mathcal{A}_o^+ is a discontinuous function at $\mathbf{e}_o = 0_3$, and it reaches infinite values in the neighbourhood of $\mathbf{e}_o = 0_3$ where \mathcal{A}_o and \mathcal{A}_o^+ approach $0_{1 \times 3}$ and $= 0_3$, respectively according to Equation (46). Therefore, utilising the Greville formula given by Equation (45) is hindered by a singularity at the steady state phase of closed loop response, and the formula cannot be used directly as a control law that enforces the algebraic SVD given by Equation (42). Instead, a singularity-free continuous GDI control law is constructed to enforce the SVD by scaling the MPGI \mathcal{A}_o^+ in the particular part of the Greville formula. The dynamically scaled generalised inverse (DSGI) is given by [23] as

$$\mathcal{A}_o^* = \frac{\mathcal{A}_o^T}{\mathcal{A}_o \mathcal{A}_o^T + v_o(t)} \tag{48}$$

where v_o is governed by the differential equation

$$\dot{v}_o(t) = -v_o(t) + k_o \frac{\|\dot{\mathbf{e}}_o\|^2}{\|\mathbf{e}_o\|^2}, \quad v_o(0) > 0, \quad k_o > 0. \tag{49}$$

The GDI attitude control law of the SGDI control system is based on the DSGI \mathcal{A}_o^* instead of the MPGI \mathcal{A}_o^+ , and is given by

$$\mathbf{u}_{\text{gdi}} = \underbrace{\mathcal{A}_o^* \mathcal{B}_o}_{\in \mathcal{R}(\mathcal{A}_o^T)} + \underbrace{\mathcal{P}_o \eta_o}_{\in \mathcal{N}(\mathcal{A}_o)}. \tag{50}$$

Unlike the MPGI \mathcal{A}_o^+ , the DSGI \mathcal{A}_o^* remains bounded [23]. Therefore, the GDI attitude control law provides robustness to the kinematical loop against MPGI singularity. The particular part $\mathcal{A}_o^* \mathcal{B}_o$ of the GDI attitude control law vanishes as $\|\dot{\mathbf{e}}_o\|$ grows, i.e. dynamic scaling of \mathcal{A}_o^+ works to deactivate the GDI attitude control loop as the attitude error variables accelerate, which drives the SLV’s kinematical subsystem to the open loop status. On the other hand, intensity of the particular part $\mathcal{A}_o^* \mathcal{B}_o$ increases by the convergence of \mathcal{A}_o^* to \mathcal{A}_o^+ as $\|\mathbf{e}_o\|$ grows, which works to re-enforce the SVD given by Equation (42). Therefore, the GDI attitude control law guarantees boundedness of the attitude error vectors \mathbf{e}_o and $\dot{\mathbf{e}}_o$, which implies robustness of the kinematical loop against closed loop instability due to environmental disturbances. Finally, although GDI is dependent on the mathematical model of the SLV, the dynamics of the scaling factor v_o is dependent only on the error measurements \mathbf{e}_o and $\dot{\mathbf{e}}_o$. Therefore, the GDI attitude control law provides robustness to the kinematical loop against closed loop instabilities due to modeling and parametric uncertainties. It follows from the expression of \mathcal{A}_o^* given by Equation (48) that $\dot{\mathbf{R}}(\mathcal{A}_o^*) = \dot{\mathbf{R}}(\mathcal{A}_o^+) = \dot{\mathbf{R}}(\mathcal{A}_o^T)$. Therefore,

$$\dot{\mathbf{R}}(\mathcal{A}_o^* \mathcal{B}_o) = \dot{\mathbf{R}}(\mathcal{A}_o^+ \mathcal{B}_o) \in \mathcal{R}(\mathcal{A}_o^T). \tag{51}$$

Hence, the GDI attitude control law preserves the geometric structure of the Greville formula. The resulting closed loop inner angular velocity dynamics is

$$\dot{\mathbf{x}}_i = \mathbf{A} + B(\mathcal{A}_o^* \mathcal{B}_o + \mathcal{P}_o \eta_o). \tag{52}$$

The full rank of the control influence matrix B implies that

$$rank(B\mathcal{P}_o) = rank(\mathcal{P}_o) = 2. \tag{53}$$

Therefore, enforcing the algebraic SVD given by Equation (42) exploits one control subspace among the three control subspaces by which the SLV’s controlled dynamics is equipped. Closing the kinematical GDI control loop by means of DSGI control guarantees boundedness of \mathbf{e} trajectories [36], but not convergence to zero, which necessitates robustifying the kinematical loop performance.

3.2 GDI inner-dynamics control loop design

The closed loop \mathbf{x}_i response changes dramatically with the design of η_o . Therefore, it is essential to design η_o in a manner that guarantees stability of the SLV's inner dynamics. To fulfill that purpose, the following inner deviation function is defined

$$\zeta = \frac{1}{2} \mathbf{x}_i^T K_i \mathbf{x}_i, \tag{54}$$

where $K_i \in \mathbb{R}^{3 \times 3}$ is a positive definite constant matrix, such that \mathbf{x}_i converges to zero if and only if ζ converges to zero. The following asymptotically stable SVD in ζ is prescribed next and is enforced by means of GDI control. The SVD takes the following linear form

$$\dot{\zeta} + b_1 \zeta = 0, \quad b_1 > 0 \tag{55}$$

such that $\zeta = 0$ is globally asymptotically stable. The first-time derivative of ζ is

$$\dot{\zeta} = \mathbf{x}_i^T K_i \dot{\mathbf{x}}_i = \mathbf{x}_i^T K_i (\Delta_i + B \mathcal{P}_o \eta_o) \tag{56}$$

where $\Delta_i = \mathbf{A} + B \mathcal{A}_o^* \mathcal{B}_o$. Hence, Equation (55) is rewritten in the following algebraic form

$$\mathcal{A}_i \eta_o = \mathcal{B}_i, \tag{57}$$

where

$$\mathcal{A}_i = \mathbf{x}_i^T K_i B \mathcal{P}_o, \tag{58}$$

and

$$\mathcal{B}_i = -\mathbf{x}_i^T K_i \Delta_i - b_1 \zeta. \tag{59}$$

Equation (57) is consistent for all $\mathbf{x}_i \neq 0_3$ and is over-determined in η_o , and therefore it has infinite number of solutions. These solutions are parameterised by an arbitrary inner null control vector $\eta_i \in \mathbb{R}^3$ in the MPGI-based Greville formula as

$$\eta_o = \underbrace{\mathcal{A}_i^+ \mathcal{B}_i}_{\in \mathcal{R}(\mathcal{A}_i^T)} + \underbrace{\mathcal{P}_i \eta_i}_{\in \mathcal{N}(\mathcal{A}_i)}, \tag{60}$$

where \mathcal{A}_i^+ is the MPGI of \mathcal{A}_i , and is given by

$$\mathcal{A}_i^+ = \begin{cases} \mathcal{A}_i^T / (\mathcal{A}_i \mathcal{A}_i^T) & \mathcal{A}_i \neq 0_{1 \times 3} \\ 0_3 & \mathcal{A}_i = 0_{1 \times 3} \end{cases} \tag{61}$$

and \mathcal{P}_i is the null projection matrix on the nullspace of \mathcal{A}_i , and is given by

$$\mathcal{P}_i = \mathbf{I}_{3 \times 3} - \mathcal{A}_i^+ \mathcal{A}_i. \tag{62}$$

The particular part $\mathcal{A}_i^+ \mathcal{B}_i$ of the null control vector η_o acts on the range space $\mathcal{R}(\mathcal{A}_i^T)$, and the auxiliary part projects η_i on the orthogonally complement nullspace $\mathcal{N}(\mathcal{A}_i)$. Because $\eta_o \in \mathbb{R}^3$ and \mathcal{A}_i^+ is a nonzero single column matrix, it follows that $rank(\mathcal{P}_i) = \dim(\eta_o) - rank(\mathcal{A}_i^+) = 3 - 1 = 2$. The expression of \mathcal{A}_i given by Equation (58) implies that $\mathcal{A}_i^T \in \mathcal{R}(\mathcal{P}_o)$. Therefore, $\mathcal{A}_o \mathcal{A}_i^T = 0$, i.e. $\mathcal{R}(\mathcal{A}_o^T)$ and $\mathcal{R}(\mathcal{A}_i^T)$ are orthogonal subspaces of \mathbb{R}^3 , $\mathcal{R}(\mathcal{P}_o)$ and $\mathcal{R}(\mathcal{P}_i)$ are also orthogonal subspaces of \mathbb{R}^3 , $\mathcal{R}(\mathcal{A}_o^T) = \mathcal{R}(\mathcal{P}_i)$, and $\mathcal{R}(\mathcal{A}_i^T) = \mathcal{R}(\mathcal{P}_o)$. Similar to the limitation of the MPGI \mathcal{A}_o^+ , the MPGI \mathcal{A}_i^+ suffers from a discontinuity at the point $\mathbf{x}_i = 0_3$, and it reaches infinite values in its neighbourhood where \mathcal{A}_i and \mathcal{A}_i^+ approach $0_{1 \times 3}$ and 0_3 , respectively. Therefore, the Greville formula given by Equation (60) cannot be used directly as a control law that enforces the algebraic SVD given by Equation (57). Following the same procedure of designing the GDI attitude control loop, a singularity-free continuous GDI control law that works to enforce the SVD is constructed by replacing the MPGI \mathcal{A}_i^+ in the particular part of the Greville formula by the DSGI \mathcal{A}_i^* given by [23]

$$\mathcal{A}_i^* = \frac{\mathcal{A}_i^T}{\mathcal{A}_i \mathcal{A}_i^T + v_i(t)} \tag{63}$$

where the dynamic scaling factor v_i is governed by the differential equation

$$\dot{v}_i(t) = -v_i(t) + k_i \frac{\|\dot{\mathbf{x}}_i\|^2}{\|\mathbf{x}_i\|^2}, \quad v_i(0) > 0, \quad k_i > 0. \tag{64}$$

The dynamically scaled outer null control law $\eta_{o_{gdi}}$ is obtained by replacing the MPGI \mathcal{A}_i^+ by the DSGI \mathcal{A}_i^* in the expression of η_o given by Equation (60), resulting in

$$\eta_{o_{gdi}} = \mathcal{A}_i^* \mathcal{B}_i + \mathcal{P}_i \eta_i. \tag{65}$$

Similar to the DSGI \mathcal{A}_o^* , the DSGI \mathcal{A}_i^* is always bounded [23]. Therefore, the dynamically scaled outer null control law $\eta_{o_{gdi}}$ provides robustness to the inner-dynamics control loop against MPGI singularity. Moreover and similar to the effect of \mathbf{u}_{gdi} on \mathbf{e}_o and $\dot{\mathbf{e}}_o$, $\eta_{o_{gdi}}$ guarantees boundedness of \mathbf{x}_i and $\dot{\mathbf{x}}_i$. Therefore, $\eta_{o_{gdi}}$ provides stability robustness to the inner-dynamics control loop against external disturbances. Finally, the dynamics of the scaling factor v_i is independent of the SLV's mathematical model and is dependent only on the angular velocity measurements \mathbf{x}_i and $\dot{\mathbf{x}}_i$. Therefore, $\eta_{o_{gdi}}$ provides robustness to the inner-dynamics control loop against instabilities due to modeling and parametric uncertainties. Because $\dot{\mathbf{R}}(\mathcal{A}_i^*) = \dot{\mathbf{R}}(\mathcal{A}_i^+) = \dot{\mathbf{R}}(\mathcal{A}_i^T)$, it follows that

$$\dot{\mathbf{R}}(\mathcal{A}_i^* \mathcal{B}_i) = \dot{\mathbf{R}}(\mathcal{A}_i^+ \mathcal{B}_i) \in \mathcal{R}(\mathcal{A}_i^T). \tag{66}$$

Hence, dynamic scaling of \mathcal{A}_i^+ does not alter the geometric structure of the Greville formula, and it follows consequently that

$$\mathcal{A}_i^{*T} \mathcal{A}_o^* = \mathcal{A}_i^{*T} \mathcal{A}_o^+ = \mathcal{A}_i^{+T} \mathcal{A}_o^+ = \mathcal{A}_i^{+T} \mathcal{A}_o^+ = 0. \tag{67}$$

Substituting the expression of $\eta_{o_{gdi}}$ given by Equation (65) in place of η_o in Equation (50) yields the SGDI control law

$$\begin{aligned} \mathbf{u}_{sgdi} &= \underbrace{\mathcal{A}_o^* \mathcal{B}_o}_{\in \mathcal{R}(\mathcal{A}_o^T)} + \underbrace{\mathcal{P}_o \eta_{o_{gdi}}}_{\in \mathcal{N}(\mathcal{A}_o)} \\ &= \underbrace{\mathcal{A}_o^* \mathcal{B}_o}_{\in \mathcal{R}(\mathcal{A}_o^T)} + \underbrace{\mathcal{P}_o (\underbrace{\mathcal{A}_i^* \mathcal{B}_i}_{\in \mathcal{R}(\mathcal{A}_i^T)} + \underbrace{\mathcal{P}_i \eta_i}_{\in \mathcal{N}(\mathcal{A}_i)})}_{\in \mathcal{N}(\mathcal{A}_o)}. \end{aligned} \tag{68}$$

The fact that $\mathcal{A}_i^T \in \mathcal{R}(\mathcal{P}_o)$ implies that $\mathcal{A}_i^* \in \mathcal{R}(\mathcal{P}_o)$ also. Hence, the projective property of \mathcal{P}_o implies that $\mathcal{P}_o \mathcal{A}_i^* = \mathcal{A}_i^*$, and the expression of \mathbf{u}_{sgdi} given by Equation (68) reduces to

$$\mathbf{u}_{sgdi} = \underbrace{\mathcal{A}_o^* \mathcal{B}_o}_{\in \mathcal{R}(\mathcal{A}_o^T)} + \underbrace{\mathcal{A}_i^* \mathcal{B}_i}_{\in \mathcal{R}(\mathcal{A}_i^T)} + \underbrace{\mathcal{P}_o \mathcal{P}_i \eta_i}_{\in \mathcal{N}(\mathcal{A}_o)}. \tag{69}$$

The fact that $\mathcal{R}(\mathcal{A}_o^*)$ is orthogonal to $\mathcal{R}(\mathcal{A}_i^*)$ implies that the two vectors $\mathcal{A}_o^* \mathcal{B}_o$ and $\mathcal{A}_i^* \mathcal{B}_i$ are always orthogonal to each other. Therefore, the dynamics of the two GDI control loops that compose the SGDI control system are independent. It follows that the order in which the two control loop closures takes place is irrelevant in designing the SGDI control system and can be performed arbitrarily. The resulting closed loop inner dynamics is

$$\dot{\mathbf{x}}_i = \mathbf{A} + B (\mathcal{A}_o^* \mathcal{B}_o + \mathcal{A}_i^* \mathcal{B}_i + \mathcal{P}_o \mathcal{P}_i \eta_i). \tag{70}$$

Because $\mathcal{R}(\mathcal{A}_o^*) \neq \mathcal{R}(\mathcal{A}_i^*)$, \mathcal{P}_o and \mathcal{P}_i project to different subspaces of \mathbb{R}^3 . Therefore,

$$\text{rank}(\mathcal{P}_o \mathcal{P}_i) = \dim(\mathbf{u}_{sgdi}) - \text{rank}(\mathcal{A}_o^*) - \text{rank}(\mathcal{A}_i^*) = 3 - 1 - 1 = 1. \tag{71}$$

The full rank of the control influence matrix B implies that

$$\text{rank}(B \mathcal{P}_o \mathcal{P}_i) = \text{rank}(\mathcal{P}_o \mathcal{P}_i) = 1. \tag{72}$$

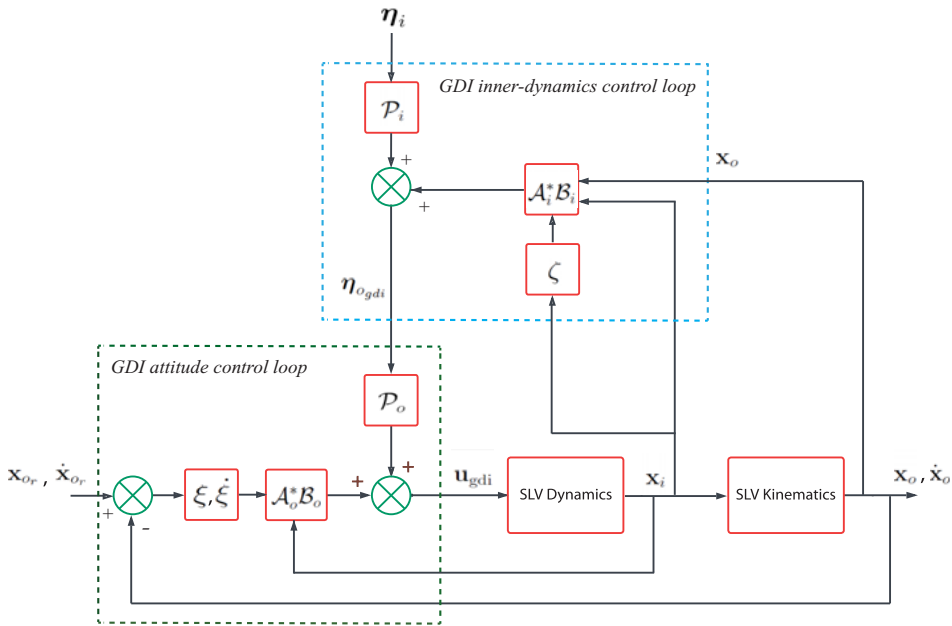


Figure 2. Baseline SGDI control system structure: detailed block diagrams of inner and outer GDI control loops and their interactions.

Therefore, enforcing the dynamical SVD given by Equation (57) exploits one additional control subspace on top of the control subspace that is exploited to enforce the kinematical SVD given by Equation (42), leaving one free control subspace among the three SLV control subspaces. The control redundancy that the third control subspace provides can be used to fulfill further objectives of the SGDI control system. Closing the inner-dynamics GDI control loop by means of DSGI control guarantees boundedness of \mathbf{x}_i trajectories [36], but not convergence, which necessitates robustifying the inner-dynamics loop performance. Actually robustifying the inner-dynamics loop performance is more important than robustifying the outer loop performance because the inner SLV dynamics given by Equation (26) is inherently dependent on the aerodynamic and inertia parameters of the SLV and on the external moments, which makes the closed loop inner dynamics of the SLV very susceptible to degradations in performance due to uncertainties in these parameters and to exogenous moment disturbances. The structure of the SGDI control system is illustrated in Fig. 2.

4.0 Performance robustification of SGDI control system

The baseline SGDI control system design guarantees boundedness of the attitude tracking error trajectories [36]. However, dynamic scalings of the MPGIs \mathcal{A}_o^+ and \mathcal{A}_i^+ , unmodeled dynamics, aerodynamic and inertia parametric uncertainties, and exogenous disturbances hinder the convergence of \mathbf{e}_o and \mathbf{x}_i . Therefore, it is necessary to robustify the SGDI control system performance against these internal and external tracking performance retardation effects.

4.1 Outer SGDI control loop design robustification

The outer loop of the baseline SGDI control system is robustified by augmenting an additional control element in the loop. Define the functional S_o as

$$S_o(\xi_o, \dot{\xi}_o, t) = \dot{\xi}_o + a_1 \xi_o + a_2 \int_{t_0}^t \xi_o d\tau, \quad t > t_0 \geq 0 \tag{73}$$

where t_0 is an initial time instant. It is obvious from Equation (73) that convergence of both ξ_o and $\dot{\xi}_o$ to zeros is equivalent to the convergence of S_o to a finite number. The time derivative of S_o is

$$\dot{S}_o = \ddot{\xi}_o + a_1 \dot{\xi}_o + a_2 \xi_o, \tag{74}$$

which can be written in the following form

$$\dot{S}_o = \mathcal{A}_o \mathbf{u} - \mathcal{B}_o. \tag{75}$$

Let us now consider the following modified kinematical SVD

$$\dot{S}_o + a_3 S_o = 0, \quad a_3 > 0. \tag{76}$$

The algebraic form of the modified kinematical SVD is

$$\mathcal{A}_o \mathbf{u} = \mathcal{B}_o - a_3 S_o. \tag{77}$$

The GDI attitude control law \mathbf{u}_{gdi} given by Equation (50) modifies accordingly to

$$\mathbf{u}_{\text{gdi}} = \underbrace{\mathcal{A}_o^* (\mathcal{B}_o - a_3 S_o)}_{\in \mathcal{R}(\mathcal{A}_o^T)} + \underbrace{\mathcal{P}_o \eta_o}_{\in \mathcal{N}(\mathcal{A}_o)}. \tag{78}$$

With the inner loop design $\eta_{o\text{gdi}}$ given by Equation (65), the SGDI attitude control law \mathbf{u}_{sgdi} given by Equation (69) modifies to

$$\begin{aligned} \mathbf{u}_{\text{gdi}} &= \underbrace{\mathcal{A}_o^* (\mathcal{B}_o - a_3 S_o)}_{\in \mathcal{R}(\mathcal{A}_o^T)} + \underbrace{\mathcal{P}_o (\underbrace{\mathcal{A}_i^* \mathcal{B}_i}_{\in \mathcal{R}(\mathcal{A}_i^T)} + \underbrace{\mathcal{P}_i \eta_i}_{\in \mathcal{N}(\mathcal{A}_i)})}_{\in \mathcal{N}(\mathcal{A}_o)} \\ &= \underbrace{\mathcal{A}_o^* (\mathcal{B}_o - a_3 S_o)}_{\in \mathcal{R}(\mathcal{A}_o^T)} + \underbrace{\mathcal{A}_i^* \mathcal{B}_i}_{\in \mathcal{R}(\mathcal{A}_i^T)} + \underbrace{\mathcal{P}_o \mathcal{P}_i \eta_i}_{\in \mathcal{N}(\mathcal{A}_o)}. \end{aligned} \tag{79}$$

The robust GDI control law \mathbf{u}_{rgdi} preserves the geometric structures of \mathbf{u}_{gdi} and \mathbf{u}_{sgdi} , i.e. the two vectors that compose \mathbf{u}_{rgdi} act on the two orthogonally complement subspaces $\mathcal{R}(\mathcal{A}_o^T)$ and $\mathcal{N}(\mathcal{A}_o)$. The resulting closed loop inner dynamics is

$$\dot{\mathbf{x}}_i = \mathbf{A} + \mathbf{B} (\mathcal{A}_o^* (\mathcal{B}_o - a_3 S_o) + \mathcal{A}_i^* \mathcal{B}_i + \mathcal{P}_o \mathcal{P}_i \eta_i). \tag{80}$$

Setting the second term on the left-hand side of Equation (76) to zero reduces the differential and algebraic forms of the modified kinematical SVD to those given by Equations (37) and (42), respectively, and reduces the the expression of \mathbf{u}_{rgdi} given by Equation (79) to that of \mathbf{u}_{sgdi} given by Equation (69). The integral action modification on the kinematical SVD aims to improve tracking performance of the GDI attitude control loop by suppressing attitude tracking errors and perturbations.

4.2 Inner SGDI control loop design robustification

The null control vector design given by Equation (65) guarantees boundedness of the SLV’s angular velocity vector. However, the GDI design of the inner loop does not guarantee convergence of the angular velocity vector, mainly because of dynamic scaling of the MPGI \mathcal{A}_i^+ . Moreover, the inner SLV dynamics given by Equation (26) is directly dependent on the aerodynamic and inertia parameters and on external moments. Therefore, the closed loop inner dynamics of the SLV is very susceptible to degradation in performance due to uncertainties in these parameters and due to exogenous disturbances.

Robust closed loop inner SGDI control system performance can be achieved in a manner that is similar to the manner followed in robustifying the closed loop outer stability of the SGDI control system,

i.e. by augmenting an additional control element in the inner loop while preserving the structure of the SGDI control law. Define the functional S_i as

$$S_i(\zeta_i, t) = \zeta_i + b_1 \int_{t_0}^t \zeta_i d\tau, \quad t > t_0 \geq 0 \tag{81}$$

where t_0 is an initial time instant. It is obvious from Equation (81) that convergence of both ζ_i and $\dot{\zeta}_i$ to zeros is equivalent to convergence of S_i to a finite constant. The time derivative of S_i is

$$\dot{S}_i = \dot{\zeta}_i + b_1 \zeta_i \tag{82}$$

which can be written in the following form

$$\dot{S}_i = \mathcal{A}_i S_i - \mathcal{B}_i \tag{83}$$

We now seek to enforce the following modified SVD on the SLV inner dynamics

$$\dot{S}_i + b_2 S_i = 0, \quad b_2 > 0. \tag{84}$$

The algebraic form of the modified dynamical SVD is

$$\mathcal{A}_i S_i = \mathcal{B}_i - b_2 S_i \tag{85}$$

Performing dynamically scaled GDI on the modified SVD given by Equation (85) yields the following expression for the differential form of the robustified GDI outer null control vector $\eta_{o\text{rgdi}}$

$$\eta_{o\text{rgdi}} = \mathcal{A}_i^* (\mathcal{B}_i - b_2 S_i) + \mathcal{P}_i \eta_i \tag{86}$$

Substituting $\eta_{o\text{rgdi}}$ in the expression of \mathbf{u}_{rgdi} given by Equation (78) yields the following robustified SGDI control vector of the SLV

$$\begin{aligned} \mathbf{u}_{\text{rgdi}} &= \underbrace{\mathcal{A}_o^* (\mathcal{B}_o - a_3 S_o)}_{\in \mathcal{R}(\mathcal{A}_o^T)} + \underbrace{\mathcal{P}_o (\mathcal{A}_i^* (\mathcal{B}_i - b_2 S_i))}_{\in \mathcal{N}(\mathcal{A}_i)} + \underbrace{\mathcal{P}_i \eta_i}_{\in \mathcal{N}(\mathcal{A}_i)} \\ &= \underbrace{\mathcal{A}_o^* (\mathcal{B}_o - a_3 S_o)}_{\in \mathcal{R}(\mathcal{A}_o^T)} + \underbrace{\mathcal{A}_i^* (\mathcal{B}_i - b_2 S_i)}_{\in \mathcal{R}(\mathcal{A}_i^T)} + \underbrace{\mathcal{P}_o \mathcal{P}_i \eta_i}_{\in \mathcal{N}(\mathcal{A}_o)} \end{aligned} \tag{87}$$

The resulting closed loop inner dynamics is

$$\dot{\mathbf{x}}_i = \mathbf{A} + B (\mathcal{A}_o^* (\mathcal{B}_o - a_3 S_o) + \mathcal{A}_i^* (\mathcal{B}_i - b_2 S_i) + \mathcal{P}_o \mathcal{P}_i \eta_i) \tag{88}$$

Setting the second term on the left-hand side of Equation (84) to zero reduces the differential and algebraic forms of the modified inner SVD to those given by Equations (55) and (57), respectively, and reduces the the expression of \mathbf{u}_{rgdi} given by Equation (87) to that of \mathbf{u}_{rgdi} given by Equation (79). Augmenting an integral element of ζ in the GDI inner-dynamics control loop works to suppress the perturbations in the angular velocity vector \mathbf{x}_i . The performance-robustified SGDI control system is illustrated in Fig. 3.

5.0 Optimal reference trajectory generation, reshaping and rational energy management

This section describes the procedure that is followed in this paper to optimise the SLV reference trajectory according to the ascent flight mission requirements and constraints. The section also highlights the need to reshape the open loop optimal reference trajectory and the strategy that is followed to fulfill that purpose. Finally, the rational energy management is described.

Table 1. Data of a four-stage SLV

Parameters	Stage-1	Stage-2	Stage-3	Stage-4
Stage's mass (kg)	11836.87	4701.7	2436.65	459.73
Stage's length (m)	5.178	2.089	2.047	4.29
Max. deflection (deg)	10.2	4	4	4
Burning time (s)	63	69	63.6	61.8

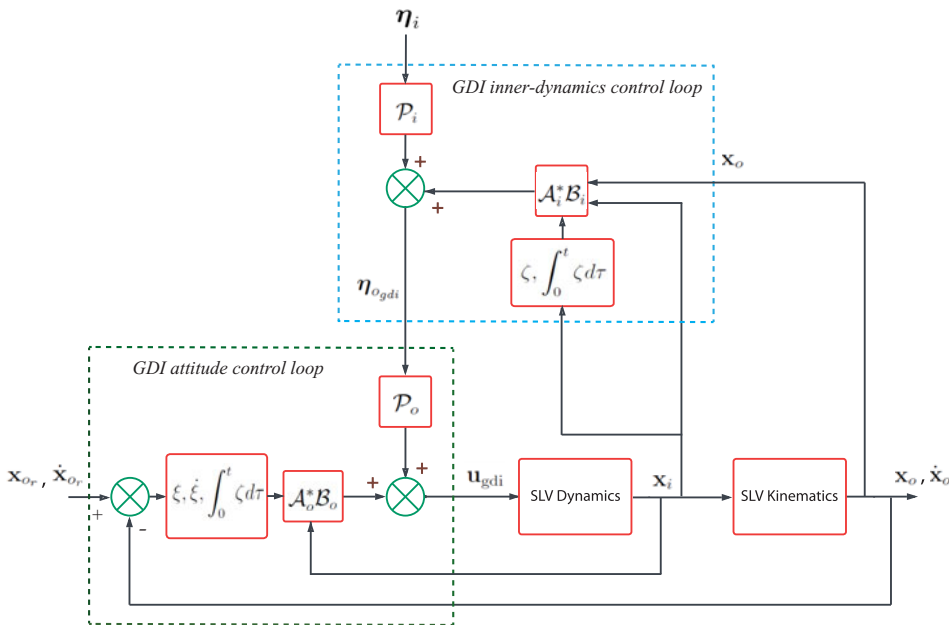


Figure 3. Robust SGDI control system structure: detailed block diagrams of robustified inner and outer GDI control loops and their interactions.

5.1 Optimal reference trajectory generation

The SLV under consideration is capable of injecting a payload of 500 kg into a 300 km sun synchronous low Earth orbit (LEO). The SLV has four stages as shown in Table 1 and was utilised in Refs. (11–13) for the purpose of SLV trajectory generation, optimisation, and control for different objectives and under different constraints.

The ascent flight of the considered SLV is composed of four burning phases, during which the SLV manoeuvres are performed by means of four engine motors. Also, the SLV experiences two coasting phases of 100 and 85 s after the second and the third stage burnouts, respectively. The ascent flight coasting phases are crucial for the SLV to attain desired orbital altitude. A schematic of the four-stage SLV's structural design is given in Fig. 4, showing stage configuration, engine motors arrangement and overall shape of the SLV. Fig. 5 depicts the operational trajectory of the present SLV ascent flight experiment and the corresponding sequence of events. The figure outlines the burning phases of each stage and the coasting phases that follow, and how these stages function sequentially during the launch process.

Generating an optimal reference trajectory for the ascent flight phase is crucial to plan for the energy that is required to fulfill the SLV mission, and to avoid excessive thrust requirements and control actuators limitations. Optimising the reference trajectory aims also to restrict aerodynamic heating on

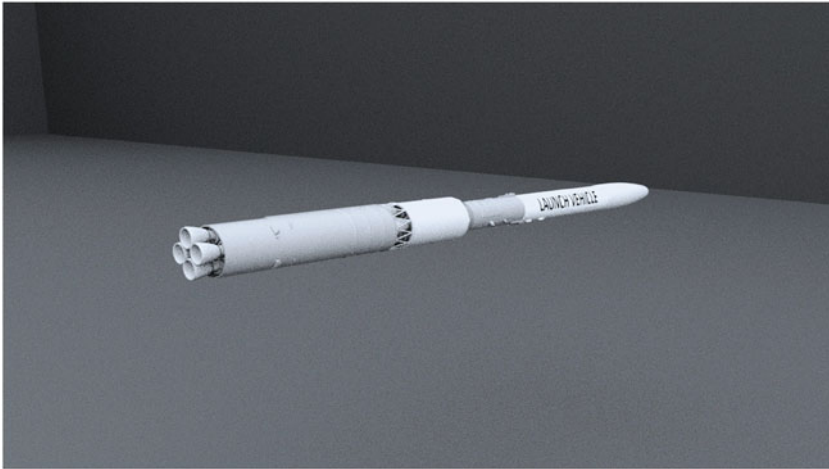


Figure 4. Four-stage SLV structural design.

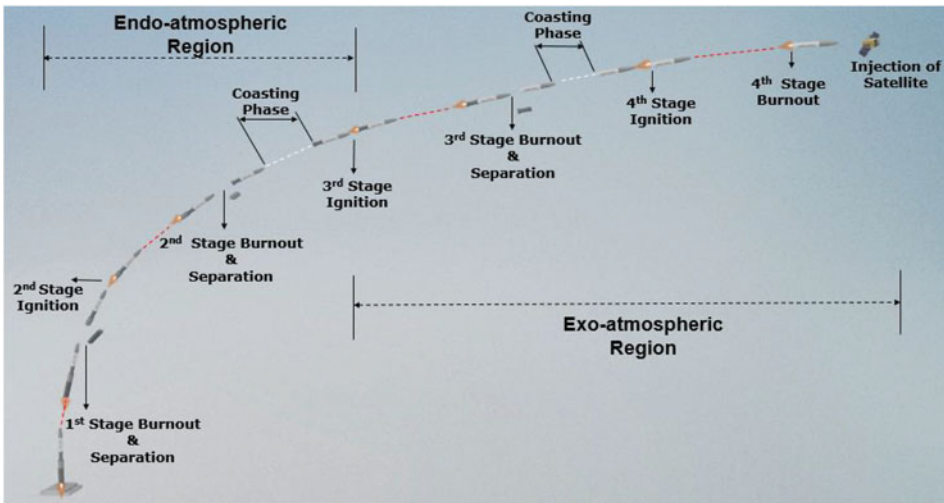


Figure 5. Four-stage SLV operational trajectory: ascent flight sequence of events and stage functionality.

the SLV’s body and to maintain its structural loading within the design limits. To generate the optimal flight trajectory, the following point mass model of the SLV is used [35]

$$\dot{\mathbf{V}}_l = \frac{L_{lb}}{m} \begin{bmatrix} T - QS_{ref}C_D \\ QS_{ref}C_{L\alpha} \\ 0 \end{bmatrix} + L_{le}\mathbf{g}_e \tag{89}$$

$$\dot{h} = \sqrt{x_e^2 + y_e^2} - R_L \tag{90}$$

$$\vartheta = \tan^{-1} \left\{ \frac{V_{yl}}{V_{xl}} \right\} \tag{91}$$

$$\theta = \alpha_{prog} + \vartheta \tag{92}$$

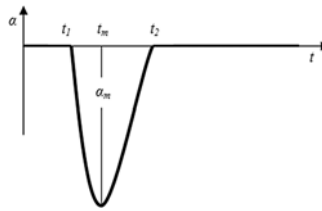


Figure 6. Designing the angle-of-attack profile: parameters t_1 , t_m , t_2 , and α_m are optimised using genetic algorithms to achieve desired orbital parameters.

where α_{prog} is the optimal angle-of-attack profile required to achieve desired orbital parameters, and R_L is the local radius of the earth given by

$$R_L = R_E \frac{1 - f}{\sqrt{1 - f(2 - f) \cos^2 \lambda}} \tag{93}$$

In the above expression of R_L , $R_E = 6378.140$ km is the Earth’s equatorial radius, $f = 0.00335281$ is the Earth’s oblateness factor, and λ is the latitude above which the point mass is located. The optimal SLV trajectory is determined by constrained optimisation of the angle-of-attack profile. The involved optimisation constraints are mainly on the maximum value of the angle-of-attack and the dynamic pressure, maximum axial and lateral inertial acceleration loadings on the body of the SLV, in addition to the orbital parameters of the mission, namely terminal velocity and altitude, and time duration of the ascent flight phase.

The design methodology that was followed to obtain the optimal SLV trajectory is based on global genetic algorithms (GA) open loop optimal guidance [11, 12]. The GA algorithm strives to find the optimal angle-of-attack profile parameters, namely the time t_1 to start the pitch-over phase, the maximum value of the angle-of-attack α_m and its occurrence time t_m , and the time t_2 at which the angle-of-attack returns back to zero as depicted in Fig. 6.

In addition to producing the optimal path to the orbit and the corresponding velocity profile, the optimal trajectory design produces the desired profiles of the pitch and yaw angles. The reference roll attitude angle is maintained at the zero value throughout the ascent flight mission. The SLV’s trajectory optimisation is performed by minimising the following objective function

$$O = (h - h_{\text{ref}})^2 + (V - V_{\text{ref}})^2 + (\vartheta_l - \vartheta_{l\text{ref}})^2, \tag{94}$$

where $h_{\text{ref}} = 300$ km, $V_{\text{ref}} = 7800$ m/s, and $\vartheta_{l\text{ref}} = 0$ deg are the corresponding reference values. Values of the parameters used in the GA implementation that yield fast convergence speed and high solution quality are shown in Table 2.

The obtained profiles of the variables that correspond to the achieved open loop optimal ascent flight phase trajectory are shown in Fig. 7.

5.2 Reference trajectory reshaping and rational energy management

The mathematical model that is usually used for the purpose of SLV trajectory generation is a simple idealised point mass model. Obtaining the point mass model requires performing several approximations and assumptions on the original six DOFs SLV model, at the cost of lowering the SLV model fidelity. Moreover, the open loop approach that is used to generate the optimal trajectory assumes undisturbed nominal environmental conditions along the SLV ascent flight trajectory.

Hence, tracking the open loop optimal trajectory leads to unsatisfactory terminal flight conditions in the presence of un-modelled SLV dynamics and external disturbances, i.e. it causes the actual values of the orbital parameters to deviate from the desired terminal constraint values. In particular, the final SLV altitude will be different from the desired orbital altitude, the orbital injection velocity will be different

Table 2. GA parameters

Parameters	Values
Generations	150
Population type	Double vector
Crossover	Single point, $pc = 0.8$
Mutation	Gaussian distribution
Reproduction	Elite count = 2
Population size	30
Termination criteria	Fitness value zero

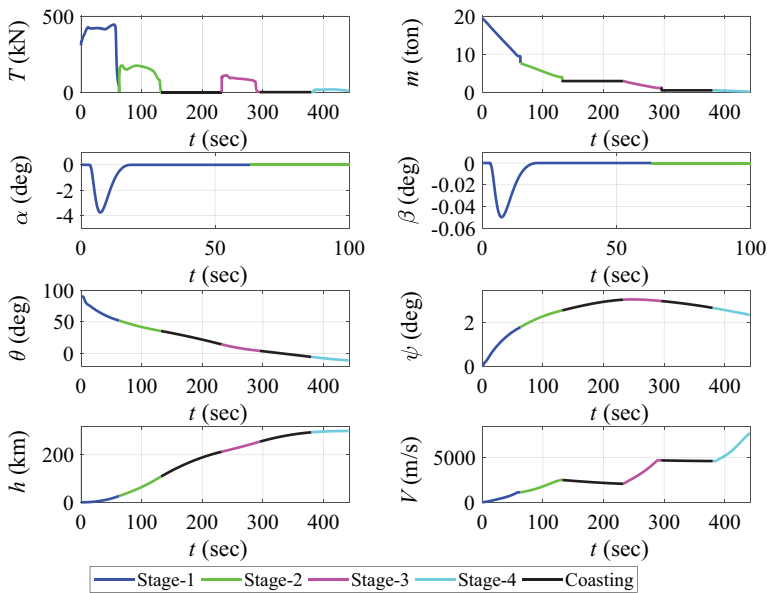


Figure 7. Optimised SLV open-loop reference trajectories: optimal parameters for different stages of the ascent flight phase versus time.

from the orbital velocity, and the orbital injection angle will be different from the desired zero flight path angle, resulting in terminal dispersions from the desired orbit.

Therefore, a realistic SLV trajectory generation design must involve a continuous in-flight updating of the open loop optimal trajectory such that the desired terminal conditions of the ascent flight phase are achieved while satisfying the mission and vehicle constraints.

To accomplish that goal, a hybrid GA/Fuzzy logic-type closed-loop guidance loop was used to reshape the generated optimal trajectory of the considered SLV and to update the reference roll and yaw commands [11, 12]. The optimal steering logic of the guidance law enhances the autonomy of the SLV by steering it closer to the pre-computed optimised reference trajectory while satisfying the mission and the vehicle constraints, in addition to satisfying the desired terminal altitude and flight path angle conditions under the influence of point mass modeling uncertainties and environmental disturbances.

Additionally, the ‘rational energy management method’ for velocity control was also suggested in Ref. (11) through activations of engine shutoff commands during the third stage powered phase to correct for the SLV velocity such that the achieved orbital injection velocity is equal to the required terminal velocity constraint despite the presence of inherent perturbations and environmental disturbances. The general structure of the closed-loop guidance and control loops is depicted in Fig. 8.

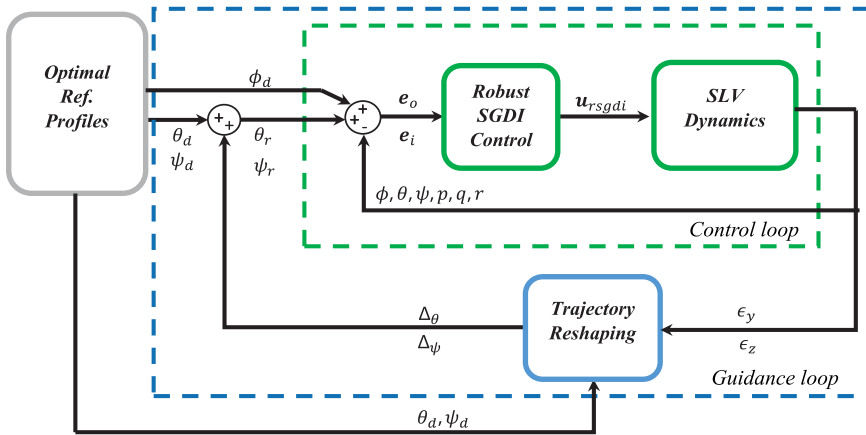


Figure 8. SLV closed-loop guidance and robust SGDI control system: reference attitude trajectories are reshaped by the guidance loop and are fed into the robust SGDI control system.

The optimal reference trajectory design provides the open loop attitude commands $\phi_d = 0, \theta_d,$ and ψ_d to the guidance (outer) loop. The trajectory reshaping mechanism is implemented to generate the closed loop reference attitude commands θ_r and ψ_r , given by

$$\theta_r = \theta_d + \Delta_\theta, \quad \psi_r = \psi_d + \Delta_\psi \tag{95}$$

where Δ_θ and Δ_ψ are computed as

$$\Delta_\theta = k_\theta \epsilon_y, \quad \Delta_\psi = k_\psi \epsilon_z, . \tag{96}$$

In (96), the normal dispersion ϵ_y is the deviation of the SLV position trajectory from its nominal path in the $x_l y_l$ plane of the LRF, i.e. $\epsilon_y = h - h_{ref}$. The lateral dispersion ϵ_z is the deviation of the SLV position trajectory from the nominal path in the transverse (normal to the $x_l y_l$ plane) direction, and k_θ and k_ψ are positive gain constants. The aim of this paper is to design the robust SGDI control system to track the closed loop reference attitude trajectories θ_r and ψ_r , while maintaining ϕ_d at zero.

6.0 Numerical simulations

The robust SGDI SLV closed loop control system simulations are carried out next with reference trajectory reshaping. To emphasise the advantage of robustifying the baseline SGDI control system via the integral term, closed loop simulations are carried out with and without the integral robustifying term for the purpose of comparing the performance of the two control laws. A comparative study follows the proposed robust SGDI control system and a classical SMC trajectory tracking control system. Finally, a statistical dispersion analysis of the robust SGDI control system is performed by extensive Monte Carlo simulations.

6.1 Robust SGDI SLV control simulations with trajectory reshaping

Numerical simulations of closed loop-controlled attitude manoeuvres along with trajectory reshaping are performed on a six DOFs SLV simulator to demonstrate the performance of robust SGDI control. The parameter values of reshaped closed loop guidance and robust SGDI control are summarised in Table 3 for different time intervals of the ascent flight.

To demonstrate the robustness attributes of SGDI control, parametric uncertainties and external perturbations are included intentionally in the mathematical model of the multi-stage SLV simulator while

Table 3. Numerical values of guidance and control parameters

Parameters	Stage-1	Stage-2	Stage-3	Stage-4
a_1	35 (<10 sec)	50	15	5
	30 (10–20 s)			
	50 (>20 s)			
a_2	25 (<10 s)	105	5	8
	35 (10–20 s)			
	105 (>20 s)			
a_3	0.5	0.5	0.5	0.1
b_1	10 (<10 s)	55	50	40
	25 (10–20 s)			
	55 (>20 s)			
b_2	0.5	0.5	0.5	0.5
k_o	0.5	0.5	0.5	0.5
k_i	0.5	0.5	0.5	0.5
k_θ	0.0005	0.0005	0.0001	0.0015
k_ψ	0.0004	0.0004	0.0004	0.0004
K_o	0.5	0.5	0.5	0.1
K_i	0.5	0.5	0.5	0.5

Table 4. Parametric uncertainties and disturbances

Parameters	Perturbation Magnitude
Specific impulse (<i>sec</i>)	2 %
Thrust misalignment (<i>deg</i>)	0.25 <i>deg</i>
Thrust offset (<i>mm</i>)	2 <i>mm</i>
Drag coefficient	6 %
Lift coefficient	10 %
Centre of pressure (<i>m</i>)	10 %
Centre of gravity (<i>m</i>)	10 %
Moment of inertia (<i>kg.m²</i>)	10 %
Atmospheric density (<i>kg/m³</i>)	10 %
Wind azimuth (<i>deg</i>)	270 <i>deg</i>

keeping these parameters at their nominal values in the SGDI control loops. The perturbed parameters and their perturbation percentages are listed in Table 4.

The aim of the robust SGDI control system is to track the reshaped attitude angle profiles of ϕ , θ and ψ by generating the control deflection commands u_ϕ , u_θ , and u_ψ . The attitude tracking history is shown in Fig. 9. Tracking is lost during the coasting phases due to the absence of thrust. However, the robust SGDI control system exhibits fast convergence towards the desired (reshaped) attitude profiles once thrust is restored. Very small oscillations are experienced in the θ and ψ reshaped reference attitude angles profiles and the corresponding actual controlled values during the final phase (4th stage) of flight because the inertia of the SLV continues to cause lateral and normal dispersions from the desired orbit as the guidance system is working to reshape the attitude reference profiles in order to eliminate these dispersions. The robust SGDI control system, however, provides excellent tracking of the reshaped attitude trajectories during the final phase.

The time history of the SLV body angular velocity components is shown in Fig. 10. The robust SGDI control system limits the angular velocity level and fluctuations throughout the flight trajectory even

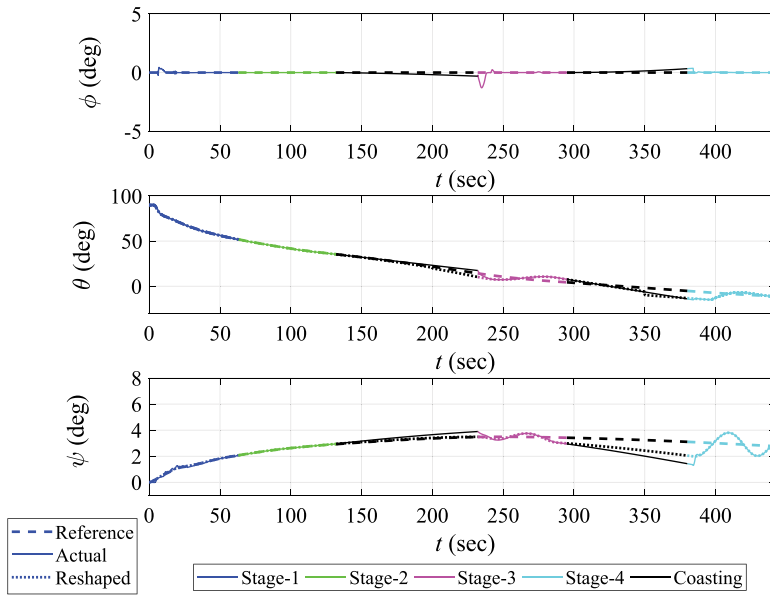


Figure 9. Robust SGDI control system performance: time histories of reference, reshaped and actual attitude angles trajectories under parametric uncertainties and wind disturbance.

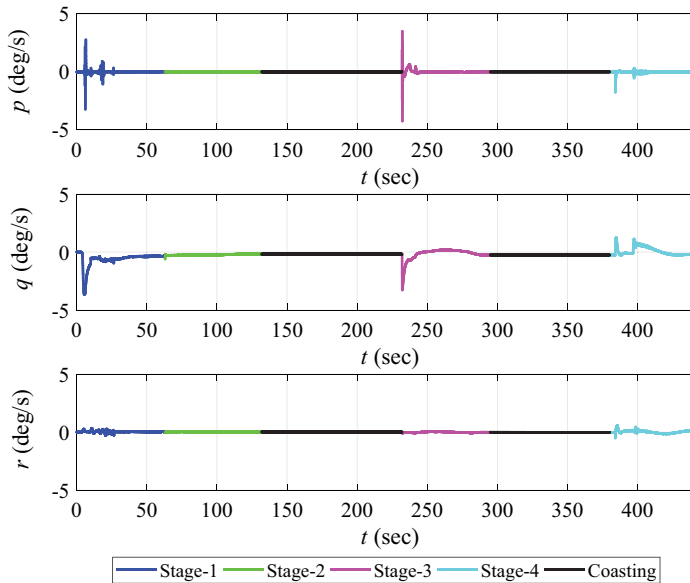


Figure 10. Robust SGDI control system performance: time histories of body angular velocity components under parametric uncertainties and wind disturbance.

in the region of high dynamic pressure, despite the inherent instability of the SLV and the presence of parametric uncertainties and wind disturbances.

The time history of the control surfaces deflection commands u_ϕ , u_θ , and u_ψ is shown in Fig. 11. The control surfaces deflections that are required to perform the attitude manoeuvres vary within a permitted

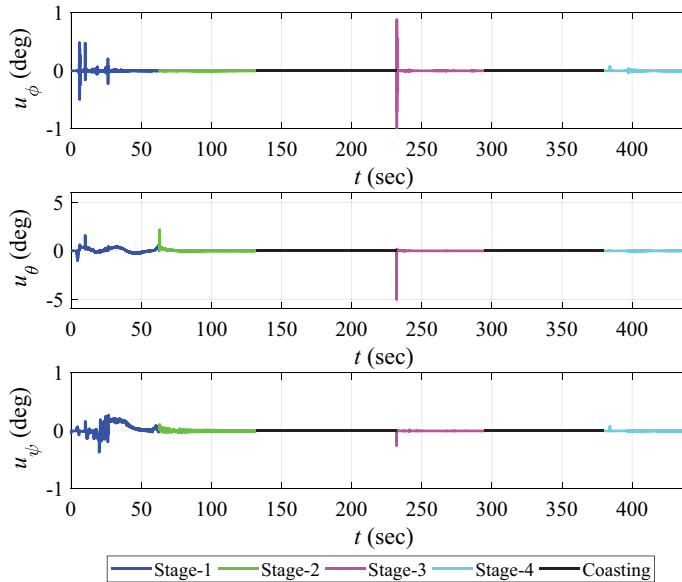


Figure 11. Robust SGDI control system performance: time histories of control surface deflections required to perform the attitude manoeuvres.

range of $\pm 5deg$, and none is experiencing undesired chattering. The control surfaces deflections are obviously zeros during the two coasting phases.

The ascent trajectory tracking performance of the SLV is depicted in Fig. 12. The SLV tracks the reference altitude profile closely as the reshaped attitude guidance commands are followed by the robust SGDI control system until the SLV achieves the desired orbit and afterwards. The positional dispersion variables ϵ_y and ϵ_z are also shown in Fig. 12. Finally, the time histories of actual and desired latitude and longitude profiles are shown in Fig. 13.

Figure 14 compares control, aerodynamic and disturbing torques due to thrust offset and misalignment throughout the ascent flight phases. Although disturbance torques are relatively small, aerodynamic torques are significant during the high aerodynamic pressure endo-atmospheric phase. The control moments effectively counterbalance these torques, maintaining stable and high-performance ascent flight.

6.2 Impact of SGDI control system robustification

In order to emphasise on the significance of robustifying the SGDI control law via the integral terms S_o and S_i , a series of comparative simulations were conducted by implementing robust SGDI control and by deliberately omitting the robustifying integral terms. The attitude variables tracking behaviours for both cases are shown in Figs 15, 16 and 17. Also, Fig. 18 shows the magnitudes of residual errors across the three attitude channels for both cases. The simulation-driven depictions highlight the distinctive impact and contribution of the SGDI robustifying terms in enhancing the overall SLV's attitude tracking performance.

The inclusion of the robustifying SGDI integral terms lead to an expedited convergence of attitude angles towards the reference attitude profiles, particularly following the coasting phases. The accelerated convergence is a clear advantage of employing robust SGDI control in improving stability robustness of SGDI control. Furthermore, it is evident that the attitude errors during the controlled powered phase are significantly reduced in the presence of the robustifying terms. The reduction of attitude tracking

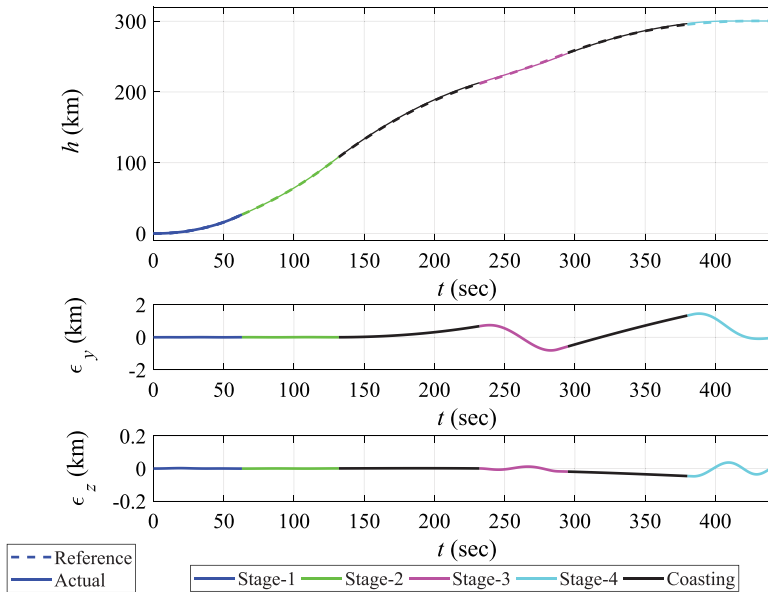


Figure 12. Robust SGDI control system performance: reference and actual altitude over time, highlighting positional dispersions.

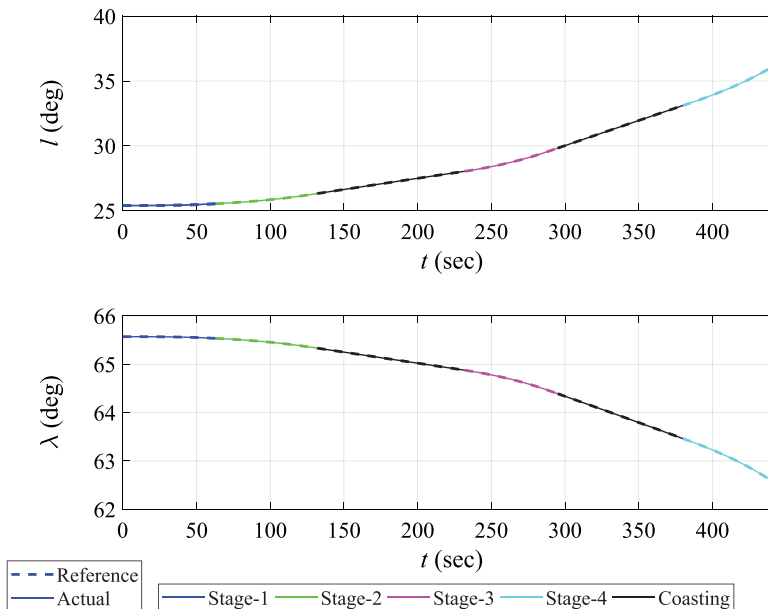


Figure 13. Robust SGDI control system performance: time histories of actual and desired latitude and longitude profiles throughout the ascent flight stages.

discrepancies substantiates the positive influence of the integral terms on performance robustness of SGDI control. Similarly, Figs 19 and 20 show the robust SGDI terms effect on the SLV’s body angular velocity and control surfaces deflections.

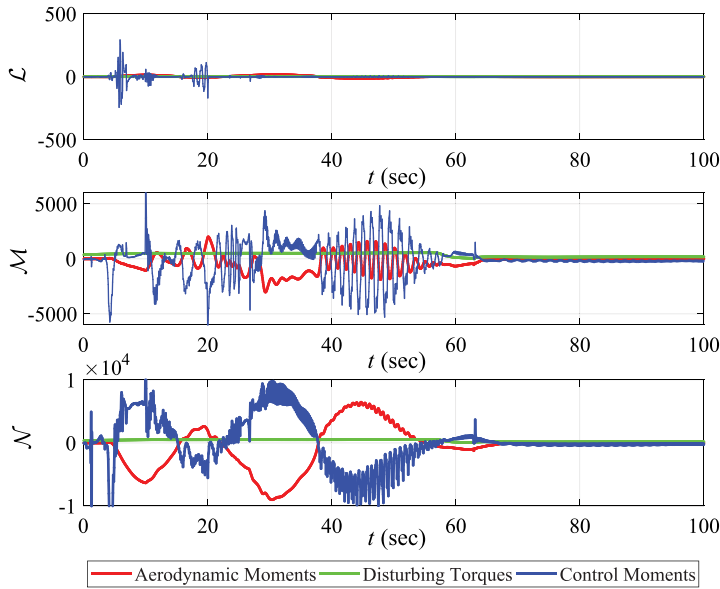


Figure 14. Robust SGDI control system performance: time histories of control moments in comparison with aerodynamic and disturbance torques, showcasing the control moments counter effects.

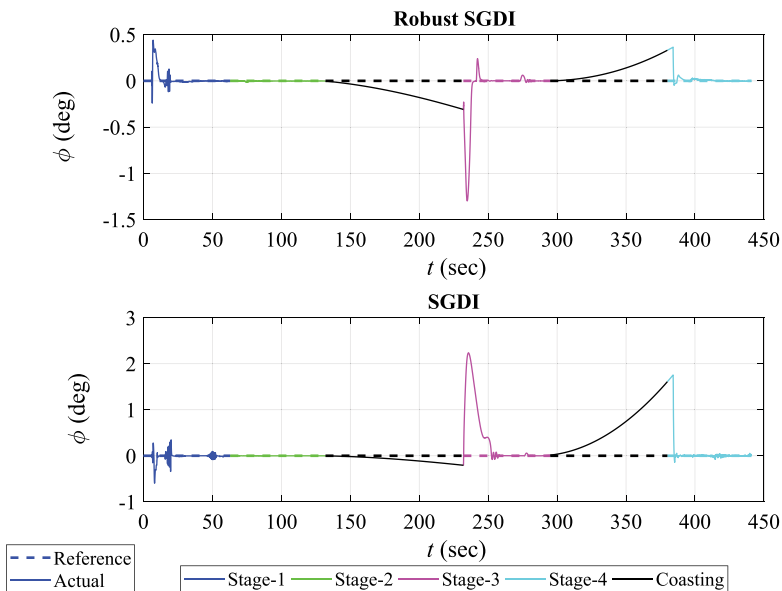


Figure 15. SGDI vs. robust SGDI: roll angle behaviour throughout ascent flight stages.

However the outer guidance loop overshadow the impact of the robust SGDI terms in the context of ascent flight trajectory. The trajectories as shown in Fig. 21 appear to follow a similar path regardless of the presence of the robustifying terms.

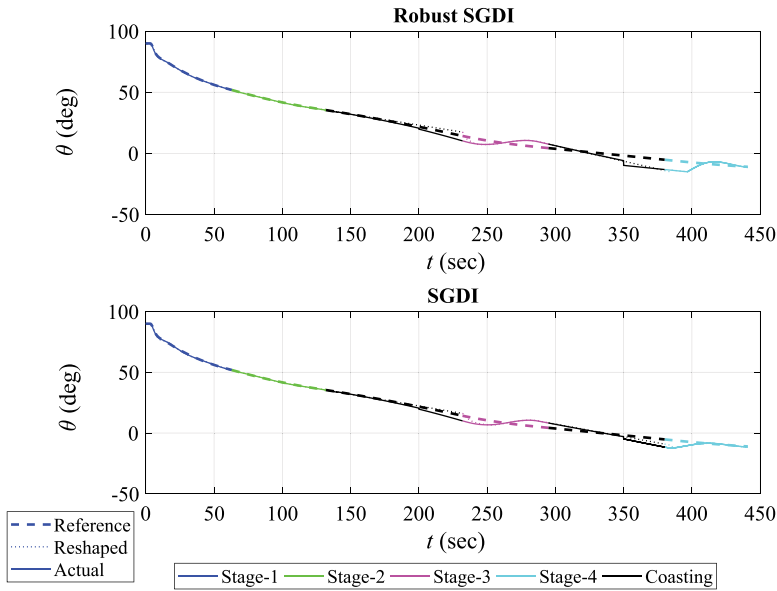


Figure 16. SGDI vs. robust SGDI: pitch angle behaviour throughout ascent flight stages.

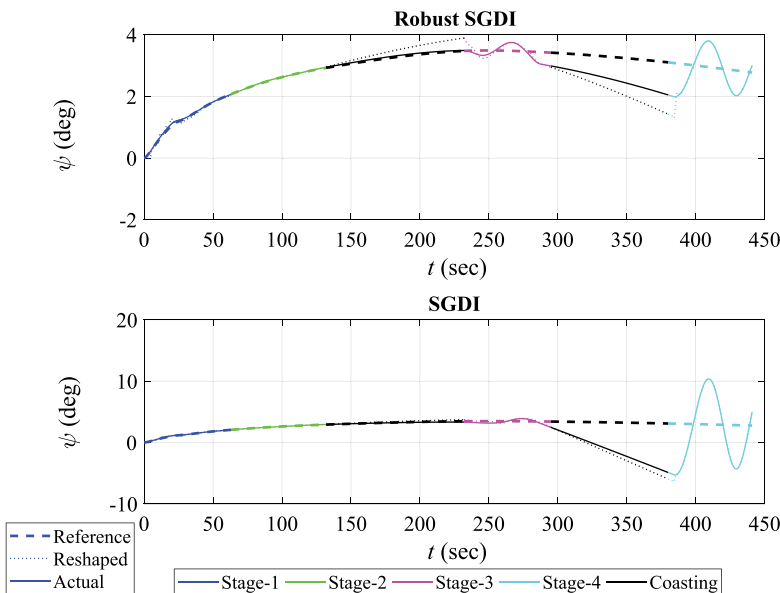


Figure 17. SGDI vs. robust SGDI: yaw angle behaviour throughout ascent flight stages.

6.3 Comparison of robust SGDI and classical SMC

The robust SGDI control system performance is assessed by comparing it with the performance of a classical SMC system, focusing on the initial pitch-over phase, which constitute approximately 100 s of the ascent flight trajectory. The comparison focuses on attitude tracking performance of both control systems during this critical phase. Time histories of attitude tracking and the corresponding square errors are shown in Figs 22 and 23, respectively.

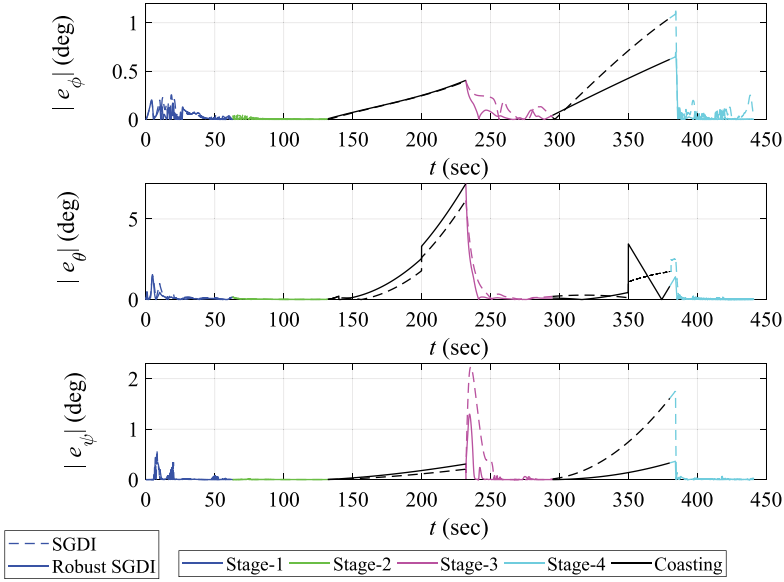


Figure 18. SGDI vs. robust SGDI: residual errors magnitudes across attitude channels throughout ascent flight stages.

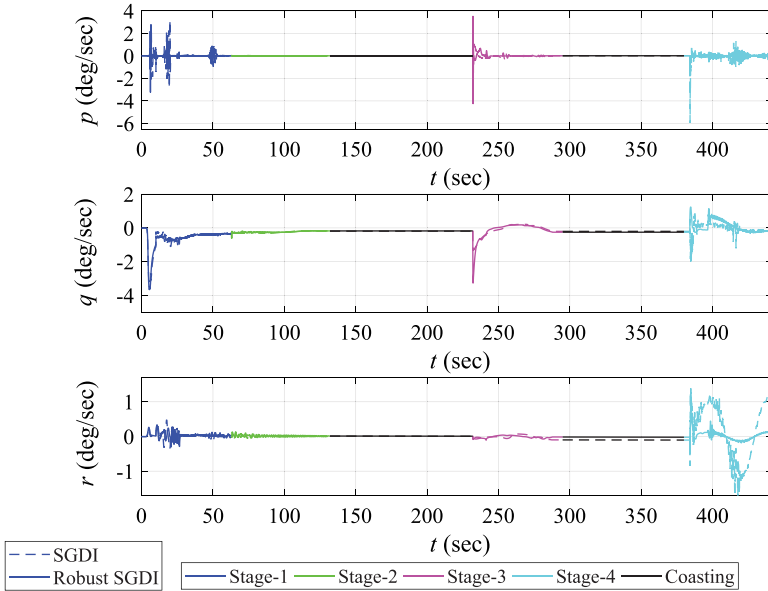


Figure 19. SGDI vs. robust SGDI: body angular velocity components throughout ascent flight stages.

With the exception of the initial 15 s for the roll channel, robust SGDI control consistently demonstrates a superior performance in minimising tracking errors when compared to SMC. Table 5 provides mean square error (MSE) and root mean square error (RMSE) comparisons for robust SGDI and SMC control across roll, pitch and yaw channels. It has been observed that robust SGDI consistently outperforms SMC in terms of MSE and RMSE, except for roll channel.

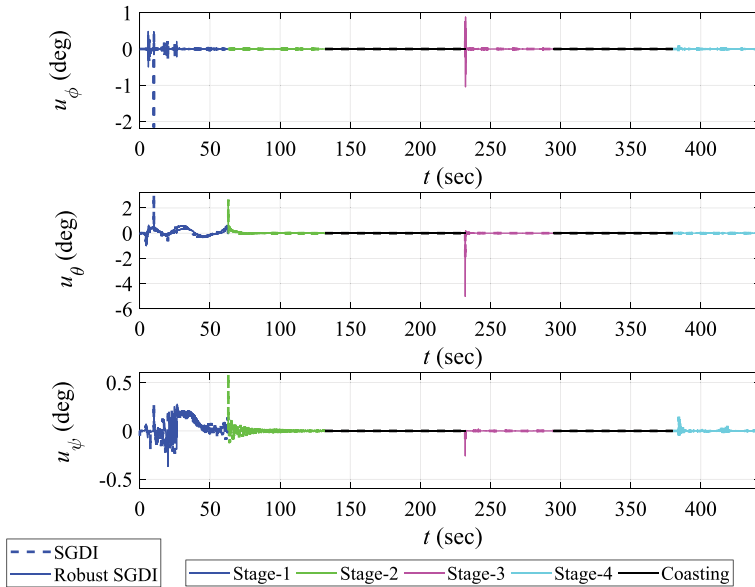


Figure 20. SGDI vs. robust SGDI: control surfaces deflections throughout ascent flight stages.

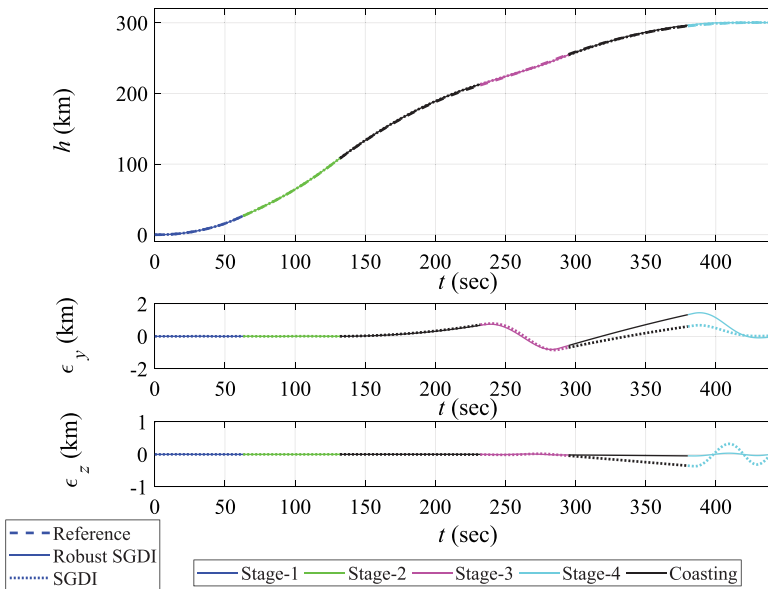


Figure 21. SGDI vs. robust SGDI: SLV's altitude throughout ascent flight stages.

Similarly, the comparison of control deflections between robust SGDI control and SMC is shown in Fig. 24. The control commands generated by SMC are impacted by the chattering phenomenon, characterised by rapid and undesirable switching behaviour of the control signal. This phenomenon can severely impede the performance and stability of the controlled system.

Table 6 provides comparisons of the control efforts required by the robust SGDI and SMC designs for attitude tracking along roll, pitch and yaw axes. The control effort for a given channel

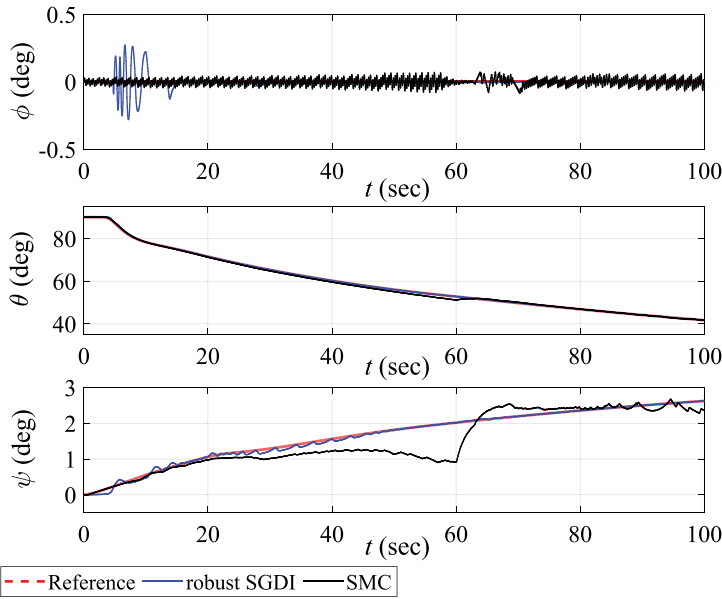


Figure 22. Robust SGDI vs. SMC: attitude tracking performance, focusing on the initial pitch-over phase of the ascent flight trajectory.

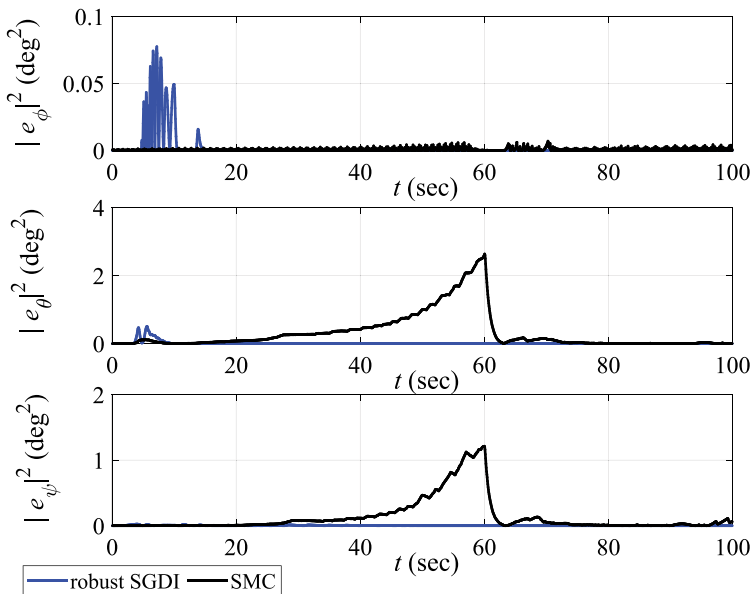


Figure 23. Robust SGDI vs. SMC: squared attitude tracking errors.

is defined as the area under the corresponding plot in Fig. 24. By examining these values, the high-performance characteristics and practicality of implementation of the robust SGDI control approach become clear.

Table 5. Attitude error comparison for robust SGDI and SMC

Parameters	Channel	Robust SGDI	SMC
Mean square error (deg^2)	Roll	0.00181	0.00075
	Pitch	0.01135	0.32234
	Yaw	0.00192	0.13453
Root mean square error (deg)	Roll	0.04258	0.02739
	Pitch	0.10653	0.56775
	Yaw	0.04385	0.36679

Table 6. Comparison of control efforts for SGDI and SMC

Channel	Control Effort: Robust SGDI (deg)	Control Effort: SMC (deg)
Roll	0.72336	28.59339
Pitch	7.30811	148.33895
Yaw	4.89253	102.76015

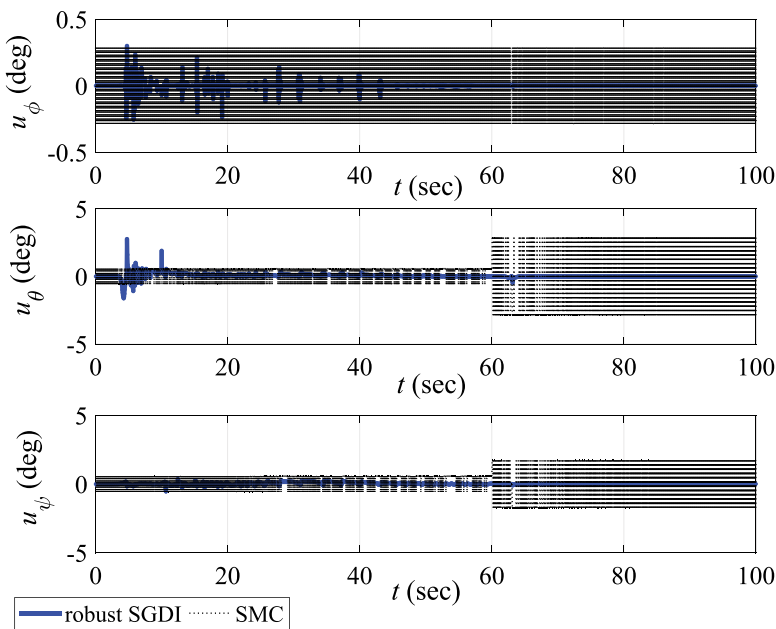


Figure 24. Robust SGDI vs. SMC: control surface deflections, revealing the SMC chattering phenomenon.

6.4 Statistical dispersion analysis of robust SGDI control

The present statistical analysis aims to investigate robustness of SGDI closed loop control with trajectory reshaping when the SLV intervenes with random variations in its dynamic parameters and under the influence of vital environmental turbulence. To accomplish this analysis, Monte Carlo simulations were conducted by considering various combinations of variations in a set of parameters that affect the SLV performance.

Table 7. Parametric variations and disturbances

Parameters	Variations
Specific impulse (<i>s</i>)	up to 2 %
Thrust misalignment (<i>deg</i>)	±0.25 <i>deg</i>
Drag coefficient	±6 %
Lift coefficient	±10 %
Centre of pressure (<i>m</i>)	±10 %
Centre of gravity (<i>m</i>)	±10 %
Atmospheric density (<i>kg/m³</i>)	±10 %
Moment of inertia (<i>kg.m²</i>)	±10 %
Wind azimuth (<i>deg</i>)	±180 <i>deg</i>

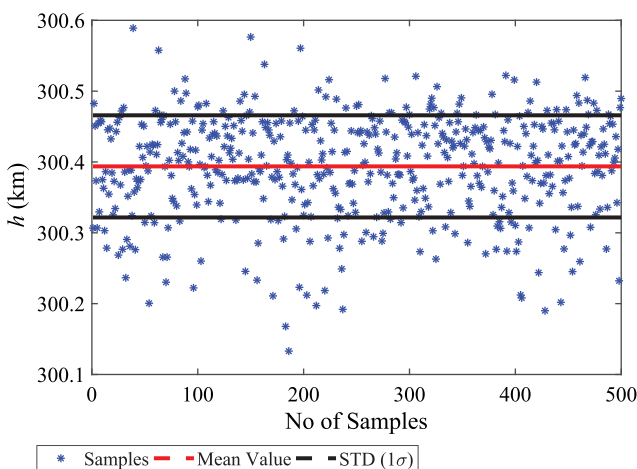


Figure 25. Monte Carlo simulations: achieved orbital altitude versus Monte Carlo simulation samples.

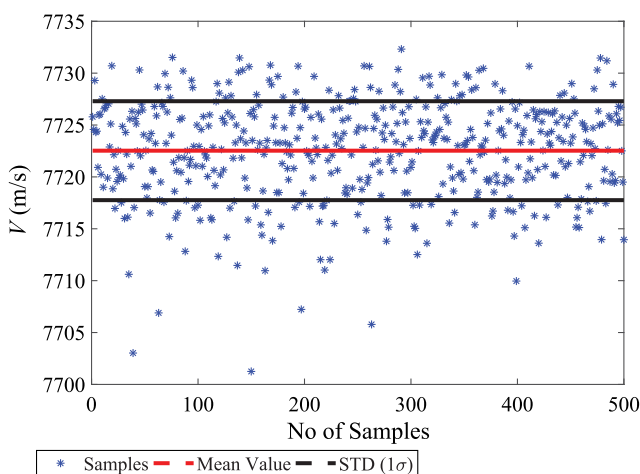


Figure 26. Monte Carlo simulations: achieved orbital velocity versus Monte Carlo simulation samples.

The parameters that are chosen to perform the Monte Carlo simulations are the specific impulse, mass flow rate, drag and lift coefficients, atmospheric density and wind azimuth. A number of 500 cases were simulated by considering an array of random variations in the chosen parameters. The variations comply

Table 8. Monte-Carlo analysis

Parameters	Nominal	Max	Mean	Standard Deviation
h (km)	300	300.58	300.39	0.07
V (m/s)	7725	7732	7722	4.76
ϑ_l (deg)	0	0.0047	0.0025	0.0007

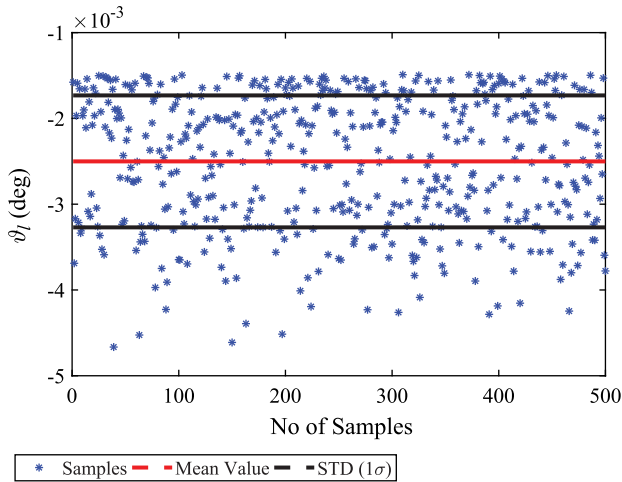


Figure 27. Monte Carlo simulations: achieved local flight path angle at orbital injection versus Monte Carlo simulation samples.

with Gaussian distributions with predefined tolerances and bounds in a specified envelope as shown in Table 7. The results acquired from Monte Carlo simulations are depicted by plotting the achieved orbital parameters against number of samples in Figs 25, 26, and 27.

The obtained dispersion data of the orbital parameters from their terminal state values using Monte Carlo simulation are depicted in Table 8, including the nominal and maximum values, the mean value and 1σ standard deviation. The achieved orbital altitude, velocity and flight path angle are within reasonable ranges and are well distributed against parametric uncertainties and environmental perturbations.

7.0 Conclusion

The paper presents a novel SGDI-based control system design for multistage SLV attitude tracking. The GDI control methodology is applied in a successive manner to design the outer and inner loops of the proposed SGDI control system, taking advantage of the favourable geometric features of GDI control. Additionally, robustifying integral control elements are augmented in the outer and inner loops of the SGDI control system to improve the SLV tracking performance against dynamic scaling of the MPGI, modeling and parametric uncertainties and exogenous disturbances. Numerical simulations are conducted on a six DOFs simulator of a four-stage SLV. The optimised reference flight trajectories are generated using genetic algorithms by employing the data of the SLV. The numerical simulations exhibit satisfactory tracking performance of the proposed robust SGDI control system by closely tracking the SLV pre-determined optimised path to achieve the required orbital parameters. The proposed robust SGDI-based control system efficiently and effectively meets the requirements of attitude control system design for multistage SLVs.

Acknowledgements. This project was funded by the Deanship of Scientific Research (DSR), King Abdulaziz University, Jeddah, Saudi Arabia, under grant no. (KEP-1-135-42). The authors, therefore, acknowledge with thanks DSR technical and financial support. This paper is part of the research work the second author did during his PhD studies at King Abdulaziz University.

Data availability. Data sharing not applicable to this article as no datasets were generated or analysed during the current study.

Competing interests. The authors declare none.

References

- [1] Reichert, R.T. Dynamic scheduling of modern robust control autopilot designs for missiles, *IEEE Control Syst. Mag.*, 1992, **12**, (5), pp 35–42.
- [2] Buschek, H. Robust autopilot design for future missile systems, In AIAA Guidance, Navigation, and Control Conference and Exhibit, New Orleans, Louisiana, USA, 1997.
- [3] Zhu, J.J., Banker, B.D. and Hall, C.E. X-33 ascent flight controller design by trajectory linearization: a singular perturbational approach, In AIAA Guidance, Navigation, and Control Conference and Exhibit, Dever, USA, 2000.
- [4] Clement, B., Duc, G. and Mauffrey, S. Aerospace launch vehicle control: a gain scheduling approach, *Control Eng. Pract.*, 2005, **13**, pp 333–347.
- [5] Steinicke, A. and Michalka, G. Improving transient performance of dynamic inversion missile autopilot by use of backstepping, In AIAA Guidance, Navigation, and Control Conference and Exhibit, California, USA, pp 46–58, 2002.
- [6] Wang, Z., Liu, L., Wang, Y. and Wang, Z. Dynamic integral sliding mode for launch vehicle attitude control system, In 24th Chinese Control and Decision Conference, Taiyuan, China, pp 1713–1718, 2012.
- [7] Das, R.K., Sen, S. and Dasgupta, S. Fault tolerant controller for attitude control of satellite launch vehicle via LMI approach, In Proceedings of the First IEEE India Annual Conference, Kharagpur, India, pp 304–309, 2004.
- [8] Das, R.K., Sen, S. and Dasgupta, S. Robust and fault tolerant controller for attitude control of a satellite launch vehicle, *IET Control Theory Appl.*, 2007, **1**, (1), pp 304–312.
- [9] Ansari, U. and Bajodah, A.H. Adaptive fuzzy sliding mode control: Application to satellite launch vehicle's attitude control. *Mechatron. Syst. Cont.*, 2018, **46**, (1), pp 15–25.
- [10] Johnson, E.N., Calise, A.J. and Corban, J.E. Adaptive fuzzy sliding mode control: Application to satellite launch vehicle's attitude control, *IEEE Aerosp. Conf. Proc.*, 2001, **6**, pp 2669–2682.
- [11] Ansari, U. Flight Vehicle Guidance and Control. School of Automation Science and Electrical Engineering, Beihang University, Beijing, China, 2007.
- [12] Ansari, U. and Alam, S. Hybrid Genetic Algorithm fuzzy rule based guidance and control for launch vehicle, In 11th International Conference on Intelligent Systems Design and Applications, Cordoba, Spain, pp 178–185, 2011.
- [13] Ansari, U. and Alam, S. Trajectory optimization and adaptive fuzzy based Launch Vehicle attitude control, In 20th Mediterranean Conference on Control & Automation, Barcelona, Spain, pp 457–462, 2012.
- [14] Pedro, J.O., Panday, A. and Dala, L. A nonlinear dynamic inversion-based neurocontroller for unmanned combat aerial vehicles during aerial refuelling, *Int. J. Appl. Math. Comput. Sci.*, 2013, **23**, (1), pp 75–90.
- [15] McFarland, M. and Hoque, S. Robustness of a nonlinear missile autopilot designed using dynamic inversion, In AIAA Guidance, Navigation, and Control Conference and Exhibit, Dever, USA, p 3970, 2000.
- [16] Valasek, J., Ito, D. and Ward, D. Robust dynamic inversion controller design and analysis for the X-38, In *AIAA Guidance, Navigation, and Control Conference and Exhibit*, Montreal, Canada, p 4380, 2001.
- [17] Doman, D.B. and Ngo, A.D. Dynamic inversion-based adaptive/reconfigurable control of the X-33 on ascent, *J. Guid. Control Dyn.*, 2002, **25**, (12), pp 275–284.
- [18] Bajodah, A.H., Hodges, D.H. and Chen, Y.H. Inverse dynamics of servo-constraints based on the generalized inverse, *Nonlinear Dynam.*, 2005, **39**, (1), pp 179–196.
- [19] Bajodah, A.H. Singularly perturbed feedback linearization with linear attitude deviation dynamics realization, *Nonlinear Dyn.*, 2008, **53**, (4), pp 321–343.
- [20] Bajodah, A.H. Generalised dynamic inversion spacecraft control design methodologies, *IET Control Theory Appl.*, 2009, **3**, (2), pp 239–251.
- [21] Bajodah, A.H. Asymptotic perturbed feedback linearisation of underactuated Euler's dynamics, *Int. J. Control*, 2009, **82**, (10), pp 1856–1869.
- [22] Bajodah, A.H. Asymptotic generalised dynamic inversion attitude control, *IET Control Theory Appl.*, 2010, **4**, (5), pp 827–840.
- [23] Hameduddin, I. and Bajodah, A.H. Nonlinear generalized dynamic inversion for aircraft manoeuvring control, *Int. J. Control*, 2012, **85**, (4), pp 437–450.
- [24] Moore, E.H. On the reciprocal of the general algebraic matrix. (*Abstract*) *Bull. Amer. Math. Soc.*, 1920, **26**, pp 394–395.
- [25] Penrose, R. A generalized inverse for matrices, *Math. Proc. Phil. Soc.*, 1955, **51**, (4), pp 406–413.
- [26] Udawadia, F.E. and Kalaba, R.E. *Analytical Dynamics: A New Approach*. Cambridge University Press, 2007.
- [27] Greville, T.N.E. The pseudoinverse of a rectangular or singular matrix and its applications to the solutions of systems of linear equations, *SIAM Rev.*, 1959, **1**, (1), pp 38–43.
- [28] Ben-Israel, A. and Greville, T.N. *Generalized Inverses: Theory and Applications*, vol. 15, Springer Science & Business Media, 2003.

- [29] Ansari, U. and Bajodah, A.H. Robust launch vehicle generalized dynamic inversion attitude control, *Aircr. Eng. Aerosp. Technol.*, 2017, **89**, (6), pp 902–910.
- [30] Ansari, U. and Bajodah, A.H. Launch vehicle ascent flight attitude control using direct adaptive generalized dynamic inversion, *Proc. Inst. Mech. Eng. G: J. Aerosp. Eng.*, 2019, **233**, (11), pp 4141–4153.
- [31] Ansari, U. and Bajodah, A.H. Robust generalized dynamic inversion based control of autonomous underwater vehicles, *Proc. Inst. Mech. Eng. M: J. Eng. Maritime Environ.*, 2018, **232**, (4), pp 434–447.
- [32] Ansari, U., Bajodah, A.H. and Hamayun, M.T. Quadrotor control via robust generalized dynamic inversion and adaptive non-singular terminal sliding mode, *Asian J. Control*, 2019, **21**, (3), pp 1237–1249.
- [33] Ansari, U., Bajodah, A.H. and Kada, B. Development and experimental investigation of a Quadrotor's robust generalized dynamic inversion control system, *Nonlinear Dyn.*, 2019, **96**, (2), pp 1541–1557.
- [34] Bajodah, A.H. Asymptotic robot manipulator generalized inverse dynamics, *Nonlinear Dyn. Syst. Theory*, 2013, **13**, (1), pp 25–46.
- [35] Xiao Y. *Rocket Ballistics and Dynamics*. Beijing University of Aeronautics and Astronautics, 2007.
- [36] Ansari, U. and Bajodah, A.H. Quadrotor control using generalized dynamic inversion and terminal sliding mode, In 5th International Conference on Control, Engineering & Information Technology, Tlemcen, Algeria, pp 1–6, 2015.